The H_2O and O_2 exospheres of Ganymede: the result of a complex interaction between the Jovian magnetospheric ions and the icy moon

Christina Plainaki [(1)], Anna Milillo [(1)], Stefano Massetti [(1)], Alessandro Mura [(1)], Xianzhe Jia [(2)], Stefano Orsini [(1)], Valeria Mangano [(1)], Elisabetta De Angelis [(1)], Rosanna Rispoli [(1)]

(1) *INAF - Istituto di Fisica dello Spazio Interplanetario Via del Fosso del Cavaliere, 00133 Roma, Italy*

(2) *Department of Atmospheric, Oceanic, and Space Sciences, University of Michigan, Ann Arbor, MI 48109-2143, USA (xzjia@umich.edu)*

Abstract

The H_2O and O_2 exospheres of Jupiter's moon Ganymede are simulated through the application of a 3D Monte Carlo modeling technique that takes into consideration the combined effect in the exosphere generation of the main surface release processes (i.e. sputtering, sublimation and radiolysis) and the surface precipitation of the energetic ions of Jupiter's magnetosphere. In order to model the magnetospheric ion precipitation to Ganymede's surface, we used as an input the electric and magnetic fields from the global MHD model of Ganymede's magnetosphere (*Jia et al., 2009*). The exospheric model described in this paper is based on EGEON, a single-particle Monte Carlo model already applied for a Galilean satellite (*Plainaki et al., 2010, 2012, 2013*); nevertheless, significant modifications have been implemented in the current work in order to include the effect on the exosphere generation of the ion precipitation geometry determined strongly by Ganymede's intrinsic magnetic field (*Kivelson et al., 1996*). The current simulation refers to a specific configuration between Jupiter, Ganymede and the Sun in which the Galilean moon is located close to the center of Jupiter's Plasma Sheet (JPS) with its leading hemisphere illuminated.

Our results are summarized as follows: a) at small altitudes above the moon's subsolar point the main contribution to the neutral environment comes from sublimated H_2O; b) plasma precipitation occurs in a region related to the open-closed magnetic field lines boundary and its extent depends on the assumption used to mimic the plasma mirroring in Jupiter's magnetosphere; c) the spatial distribution of the directly sputtered-H_2O molecules exhibits a close correspondence with the plasma precipitation region and extends at high altitudes, being, therefore, well differentiated from the sublimated water; d) the O_2 exosphere comprises two different regions: the first one is an

homogeneous, relatively dense, close to the surface thermal-O_2 region (extending to some 100s of km above the surface) whereas the second one is less homogeneous and consists of more energetic O_2 molecules sputtered directly from the surface after water-dissociation by ions has taken place; the spatial distribution of the energetic surface-released O_2 molecules depends both on the impacting plasma properties and the moon's surface temperature distribution (that determine the actual efficiency of the radiolysis process).

1 Introduction

The atmospheres of Europa and Ganymede are expected to be quite similar in composition since in both cases the surface is expected to be composed mostly of water ice and the physical conditions (temperature and moon dimensions) as well as the radiation environments are comparable. Nevertheless, Ganymede's internal magnetic field (*Kivelson et al, 1997*) makes this body unique in the Solar System. The existence of tenuous exospheres at the Galilean moons has been demonstrated through the Hubble Space Telescope (HST) Goddard High-Resolution Spectrograph (GHRS) and Advanced Camera for Surveys (ACS) observations of the Far-UV Oxygen lines, signature of dissociated molecular oxygen at Europa and Ganymede (*Hall et al., 1995; 1998; Feldman et al. 2000; Eviatar et al 2001a; McGrath et al 2004; 2013*), and through the Hydrogen Lyα line at Ganymede observed by the Galileo UV-spectrometer (*Barth et al. 1997*) and by the HST-Space Telescope Imaging Spectrograph (STIS) (*Feldman et al. 2000*), signature of neutral hydrogen.

The mechanisms expected to be predominantly responsible for the generation of a neutral environment around Ganymede are the release of surface material via direct ion sputtering and radiolysis (*Johnson et al., 2004*) and the sublimation of water ice (*Marconi, 2007*). The latter mechanism is strongly temperature dependent. The Galileo photopolarimeter (PPR) measurements (*Orton et al., 1996*) showed that Ganymede's surface temperature has a maximum value of ~150 K near the subsolar point whereas it remains constant (and equal to ~80 K) on the unilluminated hemisphere. At Europa, the measured surface temperature range is narrower (from ~86 K up to ~130 K, according to *Spencer et al., 1999*) hence the averaged expected contribution of sublimated water-ice to the moon's exospheric density is expected to be negligible. Only locally (for example at small altitudes above the subsolar point) the released fluxes due to sublimation can become comparable to those due to the other release

mechanisms (*Plainaki et al, 2010*). On the contrary, at Ganymede, the estimated surface release rate due to sublimation is expected to have a wider range of variation and a stronger spatial dependence. In particular, the contribution of this mechanism to the generation of the moon's exosphere could be substantial on the whole illuminated side (*Marconi, 2007*). Considering that water ice is the major component of the surface of an icy moon, the generated exosphere is expected to be a mixture of H_2O, O_2 and H_2 and of some other water products, such as OH and O (*Smyth and Marconi, 2006; Shematovich et al. 2005; Plainaki et al., 2012*). The spatial distribution of the exosphere of Europa is expected to depend mainly on the illumination of the moon, since its surface temperature is responsible for the efficiency of radiolysis (*Famà et al., 2008*) as well as for the sublimation rate (*Smyth and Marconi, 2006*); secondarily, the exosphere distribution depends on the ion flux that impacts the trailing hemisphere more intensively (*Pospieszalska and Johnson, 1989; Cassidy et al., 2012; Plainaki et al., 2012; 2013*). At Ganymede, the situation is expected to be more complex. In fact, the intrinsic magnetic field of Ganymede, reconnecting with the external Jovian magnetic field, partially shields the surface from the ion impact, especially at the equatorial latitudes (e.g.: *Kivelson et al, 1997*). The Jovian magnetospheric plasma at Ganymede, confined by Jupiter's magnetic field, slightly subcorotates at 150 km/s (*Scudder et al., 1981*), while the orbital velocity of Ganymede is 11 km/s (both velocities have anticlockwise direction, if seen from the North). As a result, the bulk plasma flow is constantly overtaking the satellite. The scale height of the plasma sheet at the distance of Ganymede, centered roughly around the Jovian magnetic equator, is low (*Khurana et al., 2004; 2007*); moreover, Jupiter's magnetic axis is tilted by 10 degrees with respect to its rotational axis, hence the plasma sheet oscillates up and down the satellite (*McGrath et al., 2013*). Above about 10 keV the ion flux falls off with increasing energy (*Paranicas et al. 1999*); however, these energetic particles have a significant role in the magnetosphere-moons interactions. *Mauk et al. (1996)* showed that the energy deposited on the icy satellites by magnetospheric particles is carried mainly by the particles at energies above 10 keV. The maximum ion precipitation to the surface, leading to intense sputtering and radiolysis effects, therefore, is expected to take place near the Open-Closed magnetic Field lines Boundary (OCFB) regions (e.g.: *Kivelson et al, 1997*). Eventually, the release of surface material at Ganymede is expected to depend both on the configuration of Ganymede's magnetospheric field and the illumination of the moon by the Sun. Furthermore, the dynamics of the Jovian

magnetospheric plasma control the dynamics of plasma entry into and circulation inside Ganymede's magnetosphere primarily through reconnection between Jupiter's and Ganymede's magnetic fields (*Jia et al., 2010*) and eventually determine the precipitation towards the surface (*Johnson, 1997*).

Some efforts to model Ganymede's exosphere, considering a completely collisionless neutral environment, have been already made in the past (see for example the works of *Yung and McElroy, 1977; Purves and Pilcher, 1980*). Recently, *Marconi (2007)* presented an improved 2D axisymmetric kinetic model where a simplified plasma precipitation geometry and two different cases of constant overall ion velocities (equal to 1 or 10 km/s) were considered. Moreover, these authors evaluated the generation of minor water products as a result of the interaction of the atmospheric gas mainly with photons and electrons. Ganymede's atmosphere in the *Marconi (2007)* model has been considered quasi-collisional (at altitudes < 200 km) or collisionless, while a collisional regime was assumed only in the low-altitude regions close to the subsolar point, where sublimation of water could be non-negligible. The *Marconi (2007)* model showed that close to the subsolar point (i.e. below the altitude of ~300 km), the major atmospheric species is water (with a density up to ~7 10^{14} m^{-3}); at higher altitudes, the major species is H_2 (with a density of about 10^{12} m^{-3}) while water products like OH, O and H rapidly stick onto the surface and, hence, have a minor role just below the altitude of 200 km. On the contrary, above surface regions where the plasma impact is the major release driver, two distinct atmospheric regions were revealed: at altitudes below 70 km, the O_2 is the densest species (~3 10^{14} m^{-3}) whereas above this altitude H_2 is prevailing. However, in the exosphere generation mechanisms considered in the axisymmetric model of *Marconi (2007)*, inhomogeneous surface phenomena (like temperature dependent H_2O radiolysis rate, or plasma precipitation dependent on the actual intrinsic magnetic field of the moon) were not considered. *Turc et al., 2014* confirmed the general picture given by *Marconi (2007)* results. However, comparing the results to the observations they concluded that the H density could be underestimated while the O_2 density seemed in agreement with the observations. Thus, their sublimation rates could be significantly underestimated, whereas the sputtering rates not. Furthermore, they argued that the sublimated H_2O peak in the subsolar region would disappear within one hour in the shadow of Jupiter.

The inclusion of the plasma effects (geometry and ion energy) is crucial in order to have a reliable model of the neutral environment around Ganymede. The present study

is intended to describe the 3D configuration of the major components of the exosphere in a large scale, taking into account the detailed plasma-dependent geometry and accurate simulations of the plasma – surface interactions. For this purpose we use the electric and magnetic fields from the *Jia et al. (2009)* global Magnetohydrodynamic (MHD) model of Ganymede's magnetosphere in order to perform a single-particle Monte Carlo (MC) simulation of the ions precipitation toward the moon's surface *(Section* 2); in our model, we consider only the configuration where Ganymede is located close to the center of Jupiter's Plasma Sheet (JPS). In *Section 3* we describe the exosphere simulations; we model Ganymede's neutral environment only for the configuration at which the leading hemisphere (longitude 90^0) is the illuminated one. In *Sections 3.1 and 3.2*, we describe the H_2O and O_2 exosphere sources considered in our MC model (i.e. surface sputtering and radiolysis by the energetic H^+, S^+ and O^+, and H_2O sublimation respectively). In *Section 3.3*, we describe the O_2 and H_2O exosphere loss processes and, in *Section 3.4,* we present the simulations results for the considered configuration. In *Section 4* we discuss our overall results and in *Section 5* we give the main conclusions of this work and evidence its relevance for future missions to the outer planets and their satellites.

2 Plasma precipitation to Ganymede's surface

2.1 Simulations

Hydrogen, oxygen and sulfur are the dominant ion populations of the JPS. We perform a series of Monte Carlo simulations for these populations at 1, 5, 10, 50 and 100 keV in order to describe their circulation around Ganymede and their precipitation to the moon's surface. The particle tracking is achieved via the Buneman-Boris Lorentz force integrator on the base of the magnetic and electric field data derived from the *Jia et al. (2009)* global MHD model of Ganymede's magnetosphere, which has been shown to reproduce with high fidelity the magnetic field and plasma measurements during multiple Galileo flybys of Ganymede. The set of MHD simulation data we use are computed for the orbital configuration when Ganymede is very close to the centre of JPS, in a 20×20×20 R_G simulation box, centred on the moon (with R_G = 2634 km being the moon's radius). In this paper the standard "GphiO" coordinate system is used: X is along Ganymede orbital motion (and the JPS flow direction, too), Z is along the Jupiter's spin axis, and Y points toward Jupiter. To mimic the ion flow of the JPS, which co-rotates with Jupiter faster than Ganymede along its orbit and then overtakes and embeds the moon, we place a 1 R_G thick planar source surface perpendicular to the moon's orbit,

located between X = -3 R_G and X = -4 R_G upstream of Ganymede (the standoff distance of the magnetopause is ~ 2 R_G). The source surface is subdivided in 0.2 × 0.2 R_G cells and 1000 test particles are launched with a defined initial energy but random initial direction from each cell, simulating a total of about 10^7 ions in each run.

Due to the compression of the magnetic field lines on the trailing side of Ganymede, a fraction of test particles is driven away from the Z = 0 plane, and gets quickly "lost" by crossing the top and bottom sides of the simulation box (Z = ±10 R_G). This escape leads to an underestimation of the ion circulation and the ion precipitation to the surface, since Ganymede is embedded within the JPS and then the ions are expected to (re)enter in the simulation box, bouncing back somewhere along the field lines connected to Jupiter. To perform a more realistic simulations without introducing ad-hoc assumptions, we opted to simply allow the ions to be reflected back from both the top and bottom sides (mirroring).

We run 5 different simulations for each species, namely H^+, O^+ and S^+, corresponding to energies of 1, 5, 10, 50 and 100 keV. Finally, the computed ion fluxes are scaled to the values observed by Galileo in the Ganymede's environment (*Paranicas et al., 1999)*.

Then we run also a supplementary set of simulations without mirroring. This effect could represent the case of a total loss in Jupiter's magnetosphere. It results in a lower limit case for plasma circulation around Ganymede.

2.2 Plasma precipitation results

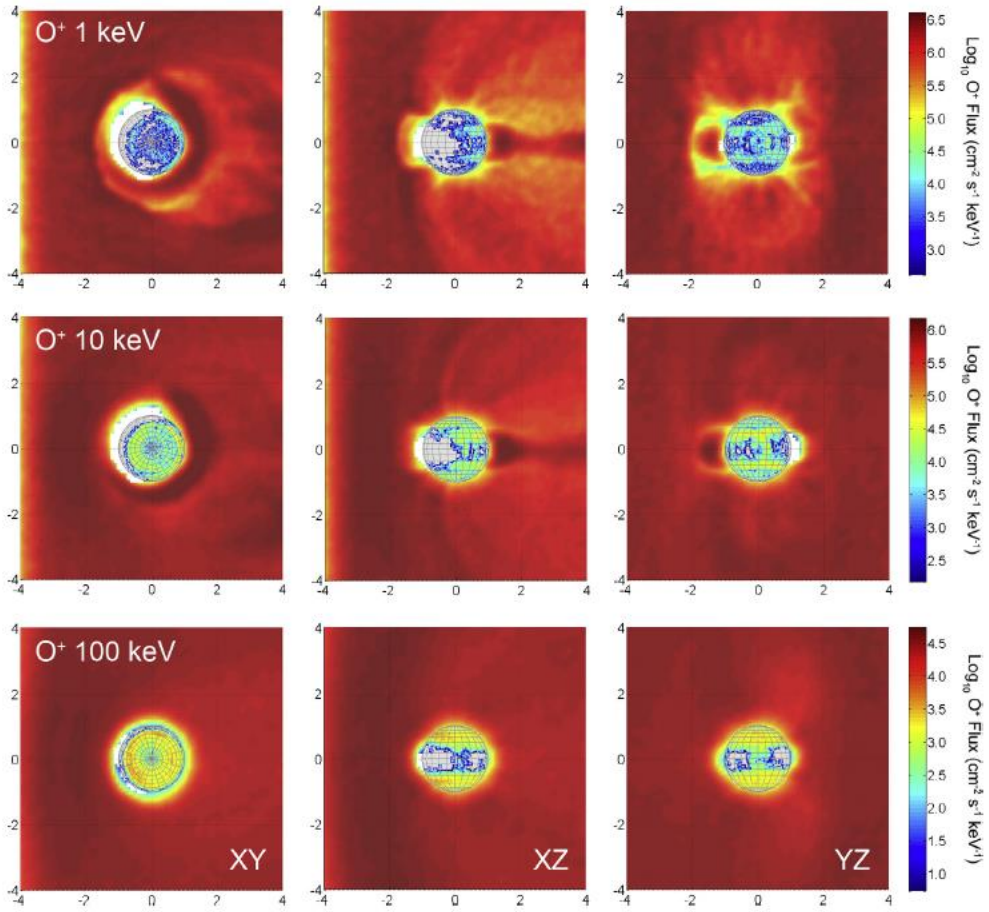

Figure 1 *shows three section (XZ, XY and YZ planes) of the O^+ ion flux computed for initial energies equal to 1, 10 and 100 keV (from top to bottom). We can see that at lower energies the magnetosphere of Ganymede can partially shield the incoming ions (coming from left in the first two columns, and towards the reader in the last one), creating a sort of bubble around the moon with reduced ion density and flux. The ion drifts around Ganymede (clockwise, as seen from the North) creates a partial torus in the equatorial plane (between about 1÷2 R_G), with higher density and flux on the trailing side, produced by ions that are bouncing back and forth along closed field lines. In this case(s) the ion precipitation on the surface is mostly focused in two belts connected with the OCFB (****Figure 2*** *left panel shows an example of an ion precipitation map corresponding to 10-keV O^+ impacting the surface). The O^+ precipitation pattern shows also that on the trailing hemisphere (apex at longitude 270°) the precipitation takes place at higher latitudes with respect to the leading hemisphere (apex at longitude 90°) where it extends to near-equator latitudes. This result is consistent with the effects of the pressure of the flowing plasma on a dipole magnetic field (Kivelson et al., 1998). In general, as the energy increases, the finite-gyroradius effect becomes more and more important (e.g., the gyroradius of 100 keV O^+ and S^+ ions is 0.70/0.25 R_G and 0.98/0.32 R_G in a magnetic field of 100/300 nT) and the 3D ion distribution becomes more and more uniform, while the ion precipitation progressively*

spreads over the whole polar caps (see, as an example,

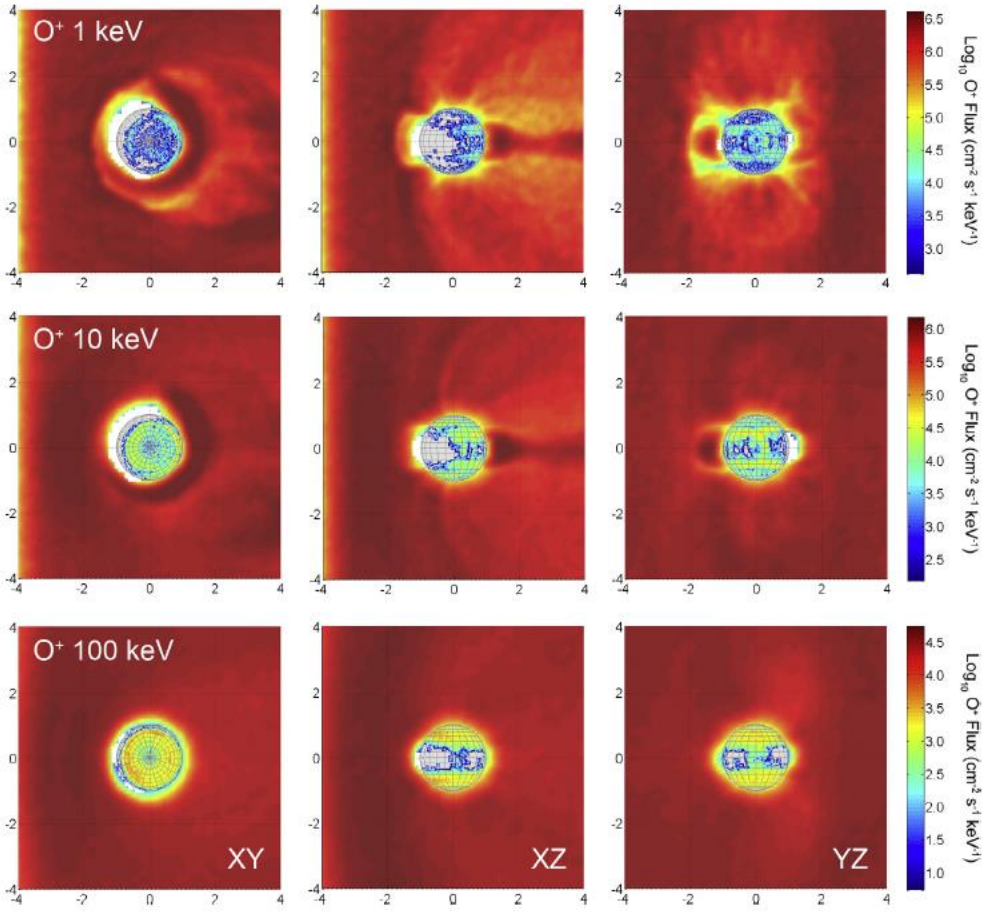

Figure 1 for the O^+ case), leaving just a low latitude belt (≤20°) generally free from ion impacts. As a rule, the precipitation regions widens out in latitudes as both the ion mass and the energy increase. The precipitating ion rates, in 5 energy ranges from 1 to 100 keV, are shown in Table *1*. The total ion precipitating rate ranges from 3.2 10^{23} s^{-1} to 6.1 10^{23} s^{-1}.

In Figure 2 (right panel), the non-mirroring case for 10-keV O^+ is presented in comparison to the mirroring one. In the former case, the expected ion precipitation is limited to two narrow rings along the OCFBs. The maximum fluxes in both cases are similar, while the total precipitating rate over the surface is considerably higher in the mirroring case.

3 The exosphere of Ganymede model

In order to simulate the effects of surface irradiation on the generation of the O_2 and H_2O exospheres around Ganymede, we implement a collisionless MC model that uses as inputs the simulated magnetospheric ion fluxes impacting the surface of the moon (see *Section 2*), considered to be composed of pure ice. The modeling technique

simulating O_2 radiolysis and sputtering is based on the previously developed Europa Global model of Exospheric Outgoing Neutrals (EGEON) (*Plainaki et al, 2010; 2012; 2013*) with a simulation box of 3x3x3 R_G and a resolution of 0.1 R_G. The H_2O sputtering simulation technique is based on the exospheric MC model of *Mura et al.* (2009) firstly applied to Mercury with spherical accumulation matrix of radius 3 R_G (resolution radial 0.1 R_G × latitude 7.5° × longitude 10°). Those models provided the 3D spatial density distribution of the main species released from the bodies' surfaces. In the current model the H_2O sublimation process is also included as described in Section 3.2. In all three simulations (O_2, sputtered-H_2O and sublimated-H_2O exospheres), each test particle has a weighing factor that is proportional to the source flux and is subjected to loss processes.

3.1 Sources: Ion Sputtering and Radiolysis

Once the magnetospheric ions precipitate on the surface of Ganymede, they can cause sputtering, ionization and excitation of water-ice molecules. Following electronic excitations and ionizations, water-ice molecules can get dissociated; chemical reactions among the water-dissociation products result in the formation of new molecules (e.g. O_2, H_2, OH and minor species) that are finally ejected from the surface into the moon's exosphere. Laboratory measurements of ice irradiation experiments have shown that H_2O molecules dominate the total release yield at lower temperatures (<120K) and O_2 and H_2 at higher (>120K) temperatures (*Johnson, 2001*). Nevertheless, any H_2 formed in ice diffuses and escapes much more efficiently than O_2 at the relevant temperatures in the outer solar system; moreover, H_2 escapes from the icy moons because of its low mass and the relatively weak gravitational fields (*Cassidy et al., 2010*). Therefore, the irradiation of Ganymede's surface can preferentially populate the magnetosphere with hydrogen, as is the case at Europa (*Lagg et al. 2003; Mauk et al. 2003*), leaving behind an oxygen-rich satellite surface (e.g., *Johnson et al. 2004*).

Release Yields

In order to calculate the H_2O and O_2 release yields (i.e. number of neutrals released after the surface impact of one ion) the model uses the formula by *Famà et al. (2008)* obtained through laboratory data fitting. In this way, our model includes the effect of surface radiation chemistry on the final release of surface molecules, avoiding the inclusion of simulations of detailed chemical processes within the icy surface. The total release yield (corresponding to the emission of H_2O, O_2, H_2) depends on the type (j)

and energy (E_j) of the impacting ion and the moon's surface temperature (T). We assume that the energy of each ion impacting the surface is E_j, i.e equal to its initial value, even if an energy gain at the surface is expected due to electric potential drop of the order of 1 mV/m (that is 2.6 keV on 1 R_G) (*Jia et al., 2009*). However, this gain is expected to be relevant only at low ion energies where the yield is lower. The yield can be written in the following form (*Plainaki et al., 2012*):

$$Y^j_{total}(E_j, T) = Y^j_{H2O}(E_j) + Y^j_{diss}(E_j, T) \quad (1)$$

where $Y^j_{H2O}(E_j)$ is the sputtering yield of the H_2O molecules, given by:

$$Y^j_{H2O}(E) = 1/U_o \cdot \left(\frac{3}{4\pi^2 C_0} a S^j_n(E) + \eta (S^j_e(E))^2\right) cos^{-f}(\vartheta) \quad (2)$$

where U_o is the surface binding energy, C_0 is the constant of the differential cross section ($d\sigma$) for elastic scattering in the binary collision approximation (*Sigmund, 1969*), a is an energy-independent function of the ratio between the mass of the target molecules and of the projectile (*Andersen et al., 1981*), S^j_n is the nuclear stopping cross section, S^j_e is the electronic stopping cross section, η is a factor that gives the proportionality between electronic sputtering and $(S^j_e(E))^2/U_o$, θ is the incidence angle, and f is an exponent of the angular dependence of the yield (*Famà et al., 2008*).

In *Eq. (1)*, $Y^j_{diss}(E_j, T)$ is the yield associated to the loss of O_2 and H_2, produced on ice after its irradiation by energetic ions and is given by :

$$Y^j_{diss}(E, T) = 1/U_o \cdot \left(\frac{3}{4\pi^2 C_0} a S^j_n(E) + \eta (S^j_e(E))^2\right) \frac{Y_1}{Y_0} e^{-\frac{E_a}{k_b T(lat,\varphi)}} cos^{-f}(\vartheta) \quad (3)$$

where Y_1 and Y_0 are fitting parameters obtained by laboratory data elaboration (see *Famà et al., 2008*), k_b is the Boltzmann constant, and *lat* and φ are the latitude and longitude respectively. However, since $Y^j_{diss}(E, T)$ has an H_2O fraction (*Teolis et al., 2010*), the assumption in *Eq. (1)* can bring some uncertainty to the calculations and therefore, the results should be evaluated with caution. Since H_2 is eventually lost from ice stoichiometrically, and since the measurements used by *Famà et al. (2008)* referred to water-equivalent molecules, the total yield for the O_2 ejection can be expressed as follows:

$$Y^j_{O2} = [m_{H2O}/(m_{O2} + 2m_{H2})] \cdot Y^j_{diss}(E_j, T) = 0.5 \cdot Y^j_{diss}(E_j, T) \quad (4)$$

where m_{H2O}, m_{O2} and m_{H2} are the molecular masses of a water, oxygen and hydrogen, respectively. The surface temperature of Ganymede determining the O_2 release yield, is assumed to be a function of the solar zenith angle, λ, as derived on the basis of the

elaboration of Galileo mission data (*Orton et al., 1996*) and considered also in *Marconi (2007)*:

$$T(\lambda) = 70 \cos(\lambda)^{0.75} + 80 \quad (5)$$

on the dayside, and $T(\lambda)$ = const =80 K on the night side. We note, however, that *Johnson et al. (1981)* discussed the possibility that the ice temperature could be significantly lower than the average disk temperature measured by the PPR instrument.

The total number (N_i) of the released molecules of type *i* depends on the product of the energy spectrum of the ion fluxes impacting the surface (*Paranicas et al., 1999*) with the energy dependent yield:

$$N_i = \int_E \sum_j dF^j/dE_j \cdot Y_i^j dE_j \quad (6)$$

where the index *j* indicates the type of the impacting ion (i.e. $j=S^+$, O^+ *or* H^+) and the index *i* indicates the released species (i.e. $i=H_2O$ or O_2).

The sputtering yields for the released H_2O molecules as a function of energy and impact ion species are shown in **Table 2**. We note that the yields increase with energy, while the impacting ion fluxes decrease. The resulting particle release is given by the product of these two quantities. However, even if the product of the yield (extrapolated at high ion energies) with the ion-flux could result in a non-negligible contribution in the surface release, the occurrence of different effects at these energies, like implantation in ice, cannot be excluded. The inclusion of impacts of ions at energies above 100 keV, at the end, can produce an overestimation of the total release. We decide to limit our energy upper limit at 100 keV.

Binding energies, sticking and bouncing

The energy of a water molecule ejected from the surface is affected mainly by the surface binding energy and secondarily by the energy or mass of the impacting ion (*Johnson, 1990*). Although the sublimation energy of H_2O is 0.45 eV/molecule, the sputtered particle energy distributions for molecular ices tend to have maxima at lower energies than a collision cascade prediction with surface binding energy equal to the normal sublimation energy (*Brown and Johnson, 1986; Boring et al., 1984; Brown et al., 1984; Haring et al., 1984*). Several explanations for this phenomenon have been proposed; the surface may be strongly disrupted with many atoms or molecules leaving at once without experiencing the same binding energy as a single atom leaving a planar surface (*Roosendaal et al., 1982; Reimann et al., 1984*). In addition, the surface region may be electronically and collisionally excited and the interatomic or intermolecular

forces are lower as a result of that excitation (*Reimann et al., 1984; Watson et al., 1983*). In this study we perform the sputtering simulation that corresponds to an 'effective' binding energy for the H_2O molecules equal to 0.054 eV, which was experimentally obtained in the past (*Boring et al. 1984, Haring et al., 1984*).

The H_2O and the O_2 molecules released from the surface are set up to ballistic trajectories until they either return to the surface of Ganymede or they escape. The number of particles used in this model is 10^5 (for the details of the Monte Carlo code see in *Plainaki et al., 2010*). Upon return to the surface, the O_2 molecules get thermalized and bounce back to continue their ballistic travel until they are either dissociated or ionized. In this model, the thermalization of the O_2 molecules upon impact with the surface, is assumed to take place immediately, as the residence time of these molecules on water ice at the relevant temperatures is typically very short compared to the ballistic flight times (*Shi et al., 2007*). The average kinetic energy that the O_2 molecules have after impacting the surface is $\sim k_b T$. The process of thermal desorption after the re-impacting of the molecules to the surface is repeated until O_2 is lost; on the contrary, upon return to the surface the H_2O molecules stick. Here we do not consider the possibility that the exospheric molecules can react with the surface. Since the lifetime (before loss) is much longer than the ballistic flight time and because most O_2 molecules are desorbed many times before loss, the majority of O_2 molecules present in the exosphere are expected to be thermal.

Energy and angular distributions

The emitted O_2 molecules have a complex energy distribution that can be considered to be mainly thermal exhibiting a high-energy tail. The distribution of the O_2 molecules that escape Ganymede's gravity is assumed to be described by an empirical function *(Johnson et al., 1983; Brown et al., 1984*) used also in previous Europa analysis (*Plainaki et al., 2012; 2013; Cassidy et al., 2007, Shematovich et al., 2005*):

$$\frac{dF}{dE_e} = a_n E_{O2}/(E_e + E_{O2})^2 \quad (7)$$

where E_{O2}*=0.015 eV* (*Shematovich et al., 2005*), a_n is the normalization factor and E_e is the energy of the ejected O_2 molecules. The ratio of the oxygen molecules escaping the moon's gravity over those released from the surface after ion impact is almost 1.6% (the O_2 escape energy at the surface is about 0.92 eV). A Maxwellian distribution function to the surface temperature is used for describing the O_2 molecules that have already had at least one contact with the surface.

The energy distribution of the ejected sputtered-water molecules considered in this model is the one given by *Sigmund (1969)*:

$$f_s(E_e, E_i) = \begin{cases} \sim \dfrac{E_e}{(E_e + E_b)^3}\left[1 - \left(\dfrac{E_e + E_b}{T_m}\right)^{1/2}\right] & E_e \le E_i - E_b \\ 0 & E_e > E_i - E_b \end{cases} \quad (8)$$

where E_e is the ejection energy, E_b, is the effective binding energy of equal to 0.054 eV *(Boring et al., 1984; Haring et al., 1984)* and T_m is the maximum energy transferred in the collision equal to $4m_i m_{H2O} E_j/(m_i + m_{H2O})^2$ (with m_{H2O} being the mass of the H_2O molecule and m_i being the mass of the impacting ion) and E_j is the energy of the impacting ion before the collision. The 'effective' surface binding energy E_b influences significantly this energy spectrum. The ratio of the water molecules escaping the moon's gravity over those released from the surface after ion impact is ~16.8% (the H_2O escape energy at the surface is about 0.52 eV).

The polar angle distribution of the sputtered particles, is generally described by a $cos^k(\varphi_e)$ law (*Hofer, 1991*), where the exponent k depends on the structure of the surface and φ_e is the ejection angle relative to the normal. In our model, we have used the assumption $k=1$ suitable for the fine-grained and porous regolith (*Cassidy and Johnson, 2005*).

3.2 Sources: Sublimation model

The contribution to the total H_2O exosphere of the sublimated molecules is estimated through the calculation of the upward flux, $F_{subl}(\lambda)$, produced at the surface of Ganymede (*Marconi, 2007*):

$$\mathrm{F_{subl}}(\lambda) = 1.1 \times 10^{31} \mathrm{T}(\lambda)^{-0.5} \exp\left(-\frac{5737}{\mathrm{T}(\lambda)}\right) \mathrm{cm^{-2} s^{-1}} \quad (9)$$

where $T(\lambda)$ is given by Eq. (5). The velocity distribution of the upward moving sublimating H_2O molecules assumed in our model is:

$$\frac{df}{dv} = \frac{n_{sub}}{(2\sqrt{\pi} T k_b/m)^2} \exp\left(-\frac{mv^2}{2Tk}\right) v dv \quad (10)$$

where n_{sub} is the density corresponding to the equilibrium sublimation pressure of H_2O (*Marconi, 2007*):

$$n_{sub} = 1.29 \times 10^{28} \exp\left(-\frac{5737}{T(\lambda)}\right) cm^{-3} \quad (11)$$

As in the case of the H_2O molecules released through sputtering, our model assumes that the sublimated molecules that return to the surface stick there and do not interact with the ice.

3.3 Losses

The main agents for the exosphere loss at a moon are the interactions taking place in its surrounding environment. Reactions in tenuous atmospheres or exospheres are dominated by the plasma interaction with neutrals and have components mainly due to a) electron impacts and b) ion-neutral charge transfer reactions. The loss rate per neutral (in units s^{-1}) is given by the ion or electron density (n_i or n_e, respectively) multiplied by a rate coefficient, κ, determined from the reaction cross section, σ, and the velocity distribution function of the ions or the electrons relative to the rest gas (*Burger et al., 2010*).

The effect of electron bombardment of the exosphere leads possibly to excitation, dissociation, and ionization; the relative importance of these reactions depends on the energies, E_{el}, of the electrons flowing through the satellite's neutral environment. For a thermalized (Maxwellian) electron population, the rate coefficient is a function of the electron temperature, T_e, since the electron thermal speeds are much larger than either the electron or neutral flow velocities. Therefore, the exosphere loss rate due to electron-impact interactions has the form (*Burger et al., 2010*):

$$v_e = n_e * \kappa(T_e) \tag{12}$$

Charge exchange processes produce exosphere losses, since thermal gas is ionized while ions at higher energy with respect to neutral gas are neutralized and mostly lost towards space. This process leads to a neutral population loss that depends on the relative bulk motion between the ions and neutrals. In case that the cross section varies slowly, or linearly, with velocity, the exosphere loss due to charge-exchange has the form (*Burger et al., 2010*):

$$v_i = n_i * v_{flow} * \sigma(v_{flow}) \tag{13}$$

where v_{flow} is the bulk flow velocity of the ions relative to the neutral gas.

At Ganymede, the properties of the Jovian magnetosphere and the characteristics of the moon's charged populations, which could be considered a tenuous ionosphere, affect the plasma-moon interactions that lead to the efficient loss of the exospheric population. In this work, we use previously published estimates of the plasma parameters of the ambient magnetospheric environment at Ganymede together with laboratory-based estimates of rate coefficients, in order to calculate the rate of the most

important interactions leading to exosphere loss. *Kivelson et al. (2004)* used Voyager-based models (*Bagenal, 1994*) and in situ measurements (*McNutt et al. 1981; Scudder et al., 1981*) in order to estimate the properties of the ambient magnetospheric plasma at Ganymede. Some information for the plasma in the moon's open field line region has also been obtained from the various Galileo flybys of Ganymede (e.g. *Gurnett et al., 1996*). *Eviatar et al. (2001b)* estimated the ionospheric (or planetary) plasma properties at Ganymede; the obtained parameter values were consistent with the upper limit predictions by *Kliore et al. (1998)*, although the plasma densities estimated by *Eviatar et al. (2001b)* were by a factor of ~5 higher than the values extrapolated by *Gurnett et al. (1996)* from the PLS measurements obtained during the Galileo G1 and G2 flybys. A summary of the physical properties of Ganymede and its surrounding plasma used in this work are presented Table *3*.

For the plasma electron energies at Ganymede (see Table *3*), the electron-impact reactions in the exosphere with the highest coefficient rates according to the data presented in *Burger et al. (2010*) are:

$$e + O_2 \text{ --> } O_2^+ + 2e \quad (14)$$

$$e + H_2O \text{ --> } OH + H + e \quad (15)$$

Considering the plasma electron density and energy at Ganymede (see Table *3*) and the coefficient rates corresponding to O_2 and H_2O reactions with electrons for this energy (*Straub et al., 1996*; *Itikawa and Mason, 2005*) we apply Eq. (12) in order to estimate the exosphere loss rate due to these processes. The average O_2 and H_2O loss rates due to electron impact are shown in **Table 4**. We note, however, that the processes (14) and (15) are expected to take place only to the exosphere regions that the plasma-electrons of the Jovian magnetosphere have access, i.e. in the open magnetic field lines regions. We underline that in our calculations we choose to consider the electron density values given by *Kivelson et al. (2004)* (and shown also in Table *3*), and we do not extrapolate the densities measured during the Galileo G1/G2 flyby to lower altitudes. This choice is justified by the suggestion by *Eviatar et al. (2001b)* that the Galileo Plasma Instrument (PLS) measurements showed approximately a constancy of the density-to-magnetic field ratio along a stream line.

In order to perform a similar estimation of the exosphere loss due to the thermal ions impacting the moon's O_2 and H_2O neutral environment, we firstly try to identify the plasma-ion properties in the near-surface region. Based on the PLS measurements taken during the Galileo G2 encounter of September 6, 1996, where Galileo passed within

261 km of the surface in the open line region, *Frank et al. (1997)* reported an outflow of protons with density 100 cm^{-3}, a bulk velocity component of ~ 70 km/s and a thermal energy of the order of 1-3 eV. However, an analysis of the Galileo Plasma Wave instrument (PWS) observations showed that the measured density should be approximately equal to the density of O_2^+ with a minor contribution of O^+ (*Eviatar et al., 2001b*). We note that the measured Galileo PWS electron densities were consistent with the PLS measurements (*Gurnett et al., 1996*). Although the report by *Frank et al. (1997)* was also consistent with the measurements reported by *Gurnett et al. (1996),* several studies indeed demonstrated that there are no protons in Ganymede's ionosphere (*Barth et al., 1997*; *Vasyliunas and Eviatar, 2000; Eviatar et al., 200b1*) and that the PLS moments assuming oxygen ions were more consistent with the electron density measurements from PWS (*Gurnett et al., 1996*) and the flow measurements inferred from the EPD (*Williams et al., 1997)* during this pass (*Jia et al., 2009*). Given the uncertainties of the identification of the near-Ganymede thermal ion environment, other authors (e.g. *Turc et al., 2014*) have chosen to partially ignore ion-neutral charge exchange processes. In this study we decide to include the loss due to the charge-exchange reactions that are due to the most important plasma ion populations in the near-Ganymede region according to *Eviatar et al. (2001b)*: O_2^+ (originating from electron-impact ionization of O_2, Eq. (14)) and O^+ (initially produced by photo-dissociation). We assume that O_2^+ is present mainly in Ganymede's polar cap region, since electron-impact dissociation of the O_2 exosphere takes place only there and in the current model we do not consider O_2^+ circulation due to Ganymede's magnetic field. In this view, the main charge-exchange reactions to be considered as loss processes in our model are:

$$O^+ + O_2 \text{ --> } O_2^+ + O \quad (16)$$

$$O^+ + H_2O \text{ --> } O + H_2O^+ \quad (17)$$

$$O_2^+ + O_2 \text{ --> } O_2 + O_2^+ \quad (18)$$

$$O_2^+ + H_2O \text{ --> } O_2 + H_2O^+ \quad (19)$$

We note that reaction (18) does not lead, directly, to a net loss of O_2, since the electron-transfer process does not result in the production of any new species accompanied by destruction of the initial species. Nevertheless, this process can result in a modulation of the exospheric O_2 energy distribution. Indeed, from the molecular oxygen point of view, Eq. (18) describes just an energization process thus favouring the gravitational escape. The quantization of this effect is hard to evaluate since we should know the

energy spectra of the O_2^+. In this model, we do not implement this energization process. Possible contribution of the H_2O^+ to a secondary exosphere loss is not considered in this study since H_2O^+ is lost via combined reactions of the ion-atom interchange and dissociative recombination of the product H_3O^+ (*Eviatar et al., 2001b*); consequently, the overall rate can be considered negligible:

$$H_2O + H_2O^+ \text{ --> } H_3O^+ + OH \quad (20)$$

$$H_3O^+ + e \text{ --> } H_2 + OH \quad (21)$$

Using Eq. (12), we calculate the coefficient rates corresponding to reactions (16) - (19) for the thermal ion energies in the Ganymede's environment and for the O_2^+ and O^+ densities given in *Eviatar et al. (2001b)*. We consider a flow velocity, v_{flow} equal to 18 km/s as inferred from the PLS observations by *Vasyliunas and Eviatar (2000)*. An upper limit of the order of ~ 25 km/s (*Eviatar et al., 2001b*) has been set from the EPD anisotropies (*Williams et al., 1998*), whereas a high conductance could lower significantly the flow velocity (*Eviatar et al., 2000*). For the reaction (16), we considered a cross section equal to $\sim 5 \cdot 10^{-17}$ cm^2 (for a O^+ velocity of 18 km/s) and equal to $\sim 10^{-16}$ cm^2 (for a O^+ velocity of 25 km/s), as measured by *Johnson et al. (2002)* and presented also in *Luna et al. (2005)*. The reactions (17) and (19) cross sections, corresponding to the velocities of interest, were taken from *Turner and Rutherford (1968)*. For the reaction (18) we used a cross section equal to $\sim 10^{-15}$ cm^2 corresponding to O_2^+ energies in the range 50-100 eV according to the recent calculations by *Benyoucef and Yousfi (2014*), a value close to those considered in other studies (e.g. *Saur et al., 1998; Marconi, 2007*).

As loss process also the effect of the photo-dissociation of O_2 and H_2O are evaluated. A summary of the estimated loss rates for all plasma-neutral reactions and photo-processes considered in this study is presented in **Table 4**.

Finally, we can conclude that the loss rate for H_2O is of the order of 10^{-5} /s in the polar caps, and of the order of 10^{-6} /s in the closed field lines regions. The exospheric O_2 net loss rate in the polar caps is in the range of $9 \cdot 10^{-8}$ - $9 \cdot 10^{-7}$ /s (the minimum value is where the electron density is lower, likely where the neutral density is higher), of the order of $\sim 10^{-7}$ /s in the illuminated side and of the order of 10^{-8} /s in the night side closed field lines regions. For simplicity we decide to assume a uniform rate of 10^{-7} /s.

In our model, we also consider the gravitational escape. As described in Section 3.1, the O_2 and the H_2O escaping fractions are about 1.6% and 16.8%, respectively.

3.4 Results

In Figure 3 we present the O_2 exosphere generated by all three species (O^+, S^+, H^+) of the magnetospheric ions impacting Ganymede's surface. As baseline scenario, we consider the case that ions get 100% reflected at ±10 R_G boundaries (mirroring) and we simulate the generated exosphere corresponding to this assumption. In this configuration the leading hemisphere (longitude 90^0) is the illuminated one; *X*-axis points to the direction of the moon's orbital velocity (also the direction of plasma flow), *Z*-axis is along Jupiter's spin axis and *Y*-axis points towards Jupiter. We note that at small altitudes above the moon's surface a thin almost homogeneous region of O_2 particles is created, whereas at higher altitudes the exospheric density is significantly lower. This tenuous homogeneous exospheric envelope has an average over the surface density of ~ $1.4 \cdot 10^{12}$ m^{-3} and is composed mainly of O_2 molecules that once thermalized to the surface temperature and released to the exosphere, had a velocity smaller than the gravitational escape velocity. Since in our model the sticking coefficient of O_2 to ice is assumed to be 0, these molecules experience numerous impacts with the surface creating this thin homogeneous envelope around Ganymede, just as it happens in the case of Europa (*Cassidy et al., 2007; Plainaki et al., 2012; 2013*). The exospheric O_2 density estimated with our model is certainly consistent with the Voyager occultation constraint of an atmospheric density less than $1.5 \cdot 10^{15}$ m^{-3} (*Broadfoot et al., 1981*).

Above the altitude of a few 100s of kms from the surface an asymmetry in the day-night O_2 exosphere is present (Figure 3, top and middle panels). At an altitude of ~0.5 R_G above the surface the day-night asymmetry in the O_2 density is up to a factor of ~47. At these altitudes, the O_2 exosphere comprises mainly the relatively energetic (i.e. not thermal) molecules that have not experienced bouncing at the surface. Therefore, the density spatial distribution at these exospheric regions reflects the surface release rate of the more energetic molecules that depends both on the moon's surface temperature and the impacting magnetospheric ion flux all over the moon. Our model shows that the high surface temperature at Ganymede's illuminated hemisphere has a major effect in the exospheric density distribution determining the actual radiolysis efficiency. Therefore, we find that the plasma precipitation distribution at the moon's surface has a less significant role (with respect to the moon's illumination) in determining the spatial distribution of the O_2 exosphere. The assumption of plasma non-mirroring in the polar cap regions leads to a decrease of the O_2 release rate by a factor of at least ~ 5.

The total surface release rate of sputtered H_2O molecules is $7 \cdot 10^{25}$ s^{-1} whereas the release rate of the sublimated H_2O is $7 \cdot 10^{29}$ s^{-1}. The sputtered-H_2O exospheric density distribution is shown in Figure 4. The sputtered-H_2O exosphere density can slightly exceed 10^{10} m^{-3} depending on the H_2O flux released through direct ion sputtering and not on the surface temperature or solar illumination. However, the sputtered H_2O flux released from the surface may have a dependence on Ganymede's orbital position since different orientations of the moon with respect to JPS could result in variations of the intensity and spatial distribution of the impacting ion flux. In the present simulation, however, we adopted a constant precipitation flux (see Section 2.1).

The H_2O exospheric density resulting from both sputtering and sublimation of water is shown in

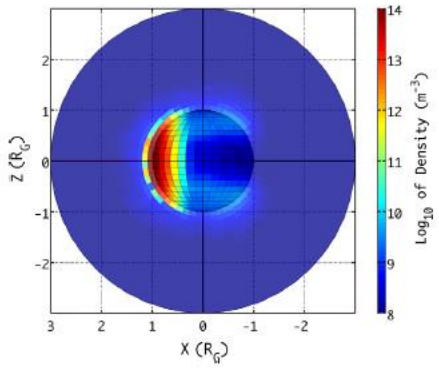

Figure 5. In this case, the position of Ganymede along its orbit is important; we have frozen the simulation at the time when the Sun is in the $+x$ direction (the illuminated side corresponds to the leading one). The exosphere density is up to ~ $2.5 \cdot 10^{14}$ m^{-3} in the sub-solar point.

The exospheric density at the surface (if we neglect the sputtering contribution, which is smaller) can be represented with the following analytical function:

$$d_0 = \exp\left(27.6 \times \cos^{0.52}(I) - 6.24\right) \tag{12}$$

The exospheric scale height is of the order of tens of km, and it is given by the following equation:

$$H = 43.3 \times \cos^{0.11}(I)\ (km) \tag{13}$$

Hence, the density in the exosphere is

$$d = d_0\, e^{-h/H} \tag{14}$$

We note that the sublimated H2O exosphere/atmosphere reaches a density that implies that the environment is no more collisionless. In

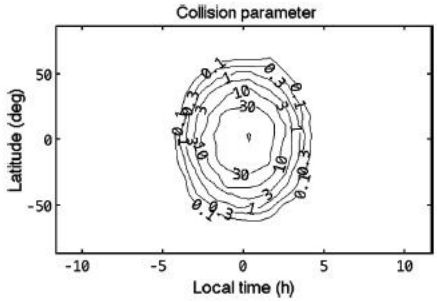

Figure 6 we plot the contour lines of the inverse of the Knudsen number, K, calculated at the surface of Ganymede. The Knudsen number is defined as $K = \ell / L$, where ℓ is the particle mean free path ($\ell = 1/(n \cdot \sigma)$ where $\sigma = 6.2 \cdot 10^{-15}$ cm^2) and L is the typical length scale considered here to be equal to the scale height (assuming both sputtering and sublimation as sources). In the hypothesis of such an intense sublimation source, the atmosphere is collisional (i.e. $1/K > 1$) in a vast area around the sub-solar point.

4 Discussion

The results of the application of our plasma circulation model show that the plasma precipitation at Ganymede occurs in a region related to the OCFB location, that is in good agreement with the Galileo magnetic field and plasma flow measurements (*Gurnett et al., 1996: Kivelson et al., 1996; 1998*). As shown in Figure 2, the extent of the plasma precipitation regions depends on the assumption used to mimic the plasma mirroring in Jupiter's magnetosphere. In particular, if mirroring is considered, the O^+ precipitation takes place inside a more extended zone that is ~ 70° wide in latitude in the trailing hemisphere. If no mirroring is considered, the O^+ precipitation is confined to a latitudinal zone that is ~10° wide and centered at the OCFB (i.e., at a latitude of ~ 50° in the North trailing hemisphere). Moreover, in the latter case, the total rate of precipitating ions is lower (see Figure 2). We note, however, that the real ion-mirroring rate is expected to have an intermediate value between 0 and 100%, since the ion population is confined inside the JPS (being partially reflected and partially lost).

At small altitudes above the regions near the subsolar point, the exosphere of Ganymede appears to include predominantly sublimated H_2O, whereas, elsewhere thermal O_2 prevails. At higher altitudes the H_2O and O_2, populations have comparable densities. The effects of the morphology of the plasma impact to the surface in the generation of the exosphere are clearly seen in the sputtered H_2O density distribution. Figure 4 shows that there is a close correspondence of the distribution of the maximum

of the sputtered H_2O exosphere density with the polar cap regions as predicted by the global MHD model of Ganymede's magnetosphere (*Jia et al., 2009*) for the case that the moon is located close to the center of JPS. Indeed, both in the northern and southern hemispheres the sputtered H_2O exospheric density maximum is located at higher latitudes in the trailing hemisphere than in the southern one. This result is not surprising, since it reproduces the trend of the OCFB described by the global MHD model of Ganymede's magnetosphere (*Jia et al., 2009*), that determines the charged particles trajectories. However, it is still very encouraging because it demonstrates that a directly sputtered neutral exospheric species can be used as a proxy for understanding the properties of the plasma impact to the moon's surface. Since Ganymede is known to have a polar cap that is brighter and bluer at visible wavelengths than the lower latitude regions (*Smith et al., 1979*), it is of crucial importance to understand its origins by examining the different candidate mechanisms (with thermal segregation and charge particle modification of the surface being the two leading explanations according to *McGrath et al., 2013*). Indeed, *Khurana et al. (2007)* noted a close correspondence between the OCFB and the boundary of the Ganymede polar cap that they interpreted as evidence that latter is associated with charged particle effects. These authors proposed that the polar caps are created by higher rates of H_2O ice sputtering at higher latitudes followed by thermal segregation of the sputtered material. Our results on the morphology of the sputtered water emission seem to support such a scenario. The full mirroring assumption results in a plasma precipitation region that is extended in latitude; consequently, in this case, primary surface sputtering takes place also at the polar regions (see Figure 7, left panel). Therefore, the mirroring scenario can on its own explain the observed higher albedo of Ganymede's polar cap. On the contrary, in the non-mirroring assumption the resurfaced regions are limited by the extension of the OCFB ring (see Figure 7, right panel); in this case, the high albedo of the whole polar cap can be explained with the action of secondary sputtering due to ionized exospheric particles that re-impact the surface of the polar regions. Further simulations that take into consideration the detailed properties of the secondary sputtering, as well as different positions of Ganymede with respect to JPS are necessary for shedding light in this direction.

The plasma effects on the exosphere generation are less evident in the O_2 density distribution, nonetheless they can still be seen in higher exospheric altitudes ($> \sim 0.2$ R_G); specifically, Figure 3 (upper panel) shows that at an altitude of ~ 0.5 R_G above the

moon's poles the density is higher by a factor of ~ 6.4 than its value at the same altitude at the night side (trailing, in this configuration) hemisphere. However, this difference in the densities is not only due to ion precipitation. O_2 particles released from the moon's illuminated hemisphere can also populate the region above the poles resulting in an increase of the exospheric density at these regions. Nevertheless, the spatial distribution of these molecules carries information related to their actual initial release from the surface (i.e. directly sputtered) since they have not been subjected to bouncing that would thermalize them after each surface impact. Therefore, Figure 3 shows that the more energetic O_2 emission has a distribution that depends both on the morphology of the plasma precipitation to the surface and on the Sun illumination that determines the efficiency of the radiolysis mechanism, in the illuminated side; indeed, the top and middle panels of Figure 3 show that at high altitudes the daylight exosphere is denser than the nightside one.

The sputtered H_2O densities obtained through the application of our model are in general in good agreement with the results obtained by *Marconi (2007)* and *Turc et al. (2014)* for the sputtering region (see upper right panel of Figure 3 in *Turc et al. (2014)*. However, in our model, the close to the surface sublimated H_2O densities (up to ~ $2.5 \cdot 10^{14}$ m^{-3}) are about an order of magnitude below their values in *Marconi (2007)* and *Turc et al. (2014)*, given for a subsolar latitude of ~ 10^0 and altitude < 50 km from the surface. In any case, this comparison is only marginal since the spatial resolution of our model, equal to ~ 0.1 R_G, is lower than the one considered in the previous models. The sublimated H_2O density is rapidly reduced with altitude in all three models; we note, however, that although the models of *Marconi (2007)* and *Turc et al. (2014)* are in good agreement between themselves up to an altitude of ~ 600 km, at higher altitudes their sublimated water densities differ by up to an order of magnitude, with those of Turc et al. been lower. The differences of our results on the sublimated H_2O exosphere in the near surface regions with the results of *Marconi (2007)* are due to the different assumptions and model spatial resolution considered in each case. Processes that can determine effectively the gas distribution of the sublimated water in the near-surface regions, such as collisions between neutrals, ion-neutral collisions and charge exchange processes, are not taken into account in our simulations. In general, near the sublimation region, the contribution of the collisions is expected to be not negligible, when Ganymede is not in Jupiter's shadow. However, even when Ganymede is not in the

shadow of Jupiter, the subsolar surface temperature considered in our simulations may not reflect the actual ice temperature, and/or the subsolar regions may be depleted in water-ice (*Pilcher et al., 1972*). Since the surface of Ganymede is a mixture of dark and light material (*Orton et al., 1996*), it is possible that the subsolar temperature of the atmospherically most important regions of water-ice may be significantly below 150 K. In such a case, the sublimation could be much less significant than what we show in Section 3.4. If sublimation is not important, the water exosphere will be globally similar to that generated through sputtering (see Figure 4).

The released O_2 density estimated with our model in the mirroring assumption is almost ~ $8 \cdot 10^{10}$ m^{-3}, at an altitude of ~ 0.15 R_G above the surface (region inside the homogeneous O_2 envelope) that is by ~ 1 order of magnitude bigger than its values in *Marconi (2007)* at this altitude, and by more than 3 orders of magnitude bigger than its values obtained by the model of *Turc et al. (2014)* (**Table 5**). We note, however, that *Marconi (2007)* considered as an input only an average (over the sputtering region) O_2 release flux equal to $1.4 \cdot 10^{13}$ m^{-2} s^{-1}; this value was chosen so as to create an O_2 column density that generates a mean disk brightness comparable to the diffuse brightness for the assumed model plasma properties. On the other hand, in order to simulate a more realistic situation, our model calculates in a dynamical way the release flux of O_2 using as inputs the spatially varying ion flux that impacts Ganymede's surface and the temperature dependent release yield. Consequently, according to our model, in the close to the surface region (< 0.1 R_G), the O_2 release flux is up to $3 \cdot 10^{14}$ m^{-2} s^{-1}, that is much higher than the considered O_2 release flux in the model of *Marconi (2007)*. The estimation of the O_2 density by *Turc et al. (2014)*, at the altitude of ~0.15 R_G, appears to be underestimated compared to both the results presented here and those presented in *Marconi (2007)*. Although *Turc et al. (2014)* and *Marconi (2007)* used the same sputtering fluxes, *Turc et al. (2014)* considered a Maxwell-Boltzman distribution (without a high energy tail) for the released O_2 assuming a collisionless regime. This choice of the energy distribution changed significantly the slope of the O_2 density profiles they obtained resulting in a rapidly decreasing O_2.

In the close to the surface region (< 0.1 R_G), where our model is less reliable, the obtained average over the surface O_2 density (equal to ~ $1.4 \cdot 10^{12}$ m^{-3}) is very close to the one derived by *Marconi (2007)* at this altitude in the sputtering region at the altitude of ~ 130 km (that is half of our model resolution equal to 0.1 R_G) and by ~2 order of

magnitude bigger than the one derived by *Turc et al. (2014)* (see **Table 5**); at altitudes even smaller than ~130 km, in the sputtering region, the O_2 densities derived with both the models of *Marconi (2007)* and *Turc et al. (2014)* are up to two orders of magnitude higher than the ones derived with our model. *Marconi (2007)* argues that O_2 is principally produced in the sputtering region via O_2^+ -O_2 interaction and not in the sublimation region. On the other hand, our model considers that the O_2 production is the result of both plasma impact and temperature dependent release mechanism. Moreover, our model does not consider dynamically collisions between neutral and ionized species (only their effect on the loss is taken into account, since we do not use a DSMC code). Such processes can populate the atmosphere and are expected to act more efficiently at near-surface altitudes since in those regions the atmosphere is denser. The model of *Turc et al. (2014)*, however collisionless, considered as inputs the same initial surface release fluxes of *Marconi (2007)*, which in any case were assumed to be spatially constant. As a result, their model tends to overestimate locally the O_2 density in the low-altitude regions since it considers the emission rate homogeneous all over the surface regions.

The most important difference between our model and both the models of *Marconi (2007)* and *Turc et al. (2014)* is the consideration, in our case, of a spatially varying ion precipitation. In our model we have reliable simulations of the ions impact to the surface, and in this way we have determined the regions from where H_2O and O_2 are released through sputtering and radiolysis, respectively.

The H_2O and O_2 escape rates calculated on the basis of the results of our model are ~ $1.3 \cdot 10^{25}$ $s^{-1}$and ~$4.2 \cdot 10^{26}$ s^{-1} respectively. Regarding the H_2O escape rate, our estimation is by a factor of ~4 higher than its value in *Turc et al. (2014)* and very close to its value in *Marconi (2007)*, equal to $1.6 \cdot 10^{25}$ s^{-1}. The first difference is due to the locally higher release rate considered in our model whereas the second difference is due to the assumptions of collisions in *Marconi (2007)* that can increase the particle escape probability. Regarding the O_2 escape rate, our estimation is higher than its value in *Marconi (2007)* by a factor of ~ 6; instead the O_2 escape rate estimated by *Turc et al. (2014)* is largely underestimated with respect to both of the other two models. The difference of our estimate with the one by *Marconi (2007)* is mainly due to the different escape mechanisms considered in each model. In our model, the escape is gravitational and it is the direct result of an energy distribution function that includes a high-energy

tail (see Eq. (7)). On the other hand, in the model by *Marconi (2007)* a thermal energy distribution is assumed for O_2; however, charge exchange reactions between O_2 and O_2^+ and ion-neutral elastic collisions can give rise to the initially thermal energy distribution leading to O_2 escape.

Numerous UV observations of the O 1304 and 1356 Angstrom emissions at Ganymede (*Hall et al., 1998; Feldman, 2000; McGrath et al., 2013*) have demonstrated a non-uniform brightness distribution over the moon (for a detailed review see in *McGrath et al., 2013*). The observations of this kind are a proxy for the existence of a O_2 neutral environment, since the respective emissions are due to electron impact dissociative excitation of molecular oxygen. Among the important findings based on the UV observations, we underline the following main points: the location of the brightest emission occurs at significantly higher latitude on the trailing /upstream hemisphere than on the leading/downstream hemisphere; the auroral emission is not symmetric about the equator in the North-South direction neither about the sub-Jupiter and anti-Jupiter facing hemispheres. The regions of peak brightness in the northern and southern hemispheres have been associated with the cusps (*Paty and Winglee, 2004*). We note, however that the HST observations are always observations of the illuminated hemisphere. We can perform a direct speculation on the consistency of the morphology of the O_2 exosphere (derived from our simulations where the leading hemisphere is illuminated) with the O emission patterns (derived from the observations) only for the HST observations of Ganymede's leading hemisphere (for example, the observations of the moon's leading hemisphere, presented in *Feldman et al. (2000)* and analyzed also in *McGrath et al. (2013)*). Our results (see Figure 3, lower panel) show that in the O_2 exosphere at the equatorial *YZ* plane, no asymmetry between sub-Jupiter and anti-Jupiter facing hemisphere is present; therefore it is likely that the observed asymmetry in the morphology of the auroral atomic O emission is due to the asymmetric precipitation of the electrons and not due to the actual exosphere density distribution. Therefore, our results for this configuration between Ganymede-Jupiter and the Sun support the scenario that the electron precipitation is the main agent that determines the spatial distribution of the atomic oxygen auroral emission at the Ganymede. However, the contribution of an inhomogeneous O_2 exosphere to the phenomenon cannot, in general, be ruled out. In absence of in situ observations in the not-illuminated side, the scenario that an asymmetric UV emission could result from the symmetry in the O_2 density distribution (as the one presented in the middle panel of Figure 3 between the

illuminated and dark exosphere) cannot be excluded. Observation during future missions at Ganymede will shed light in these investigations. In the meanwhile, a realistic description of the plasma electron distribution around Ganymede is required for any further speculation. A better understanding requires further modeling, including also other configurations between Ganymede, Jupiter and the Sun. Further data analysis is crucial in this context.

For the considered configuration we derive also the O_2 column densities, N_{O2}, at the Sun-moon and anti-Sun-moon directions in the equatorial plane. In the illuminated side, the computed column density is N_{O2}=4.2·10^{17} m^{-2}. This value is by a factor of ~2.4 lower than the lower limit of the estimations by *Hall et al. (1998)*, who combined the HST measurements of brightness, the Voyager Ultraviolet Spectrometer measurements and the Galileo electron distribution measurements above Ganymede's polar cap and computed an O_2 column density ranging from 1 to 10·10^{18} m^{-2}. In the dark side, the computed column density is N_{O2}=3.9·10^{17} m^{-2}. The underestimated value with respect to the observed one could be partially due to the limitation of our simulations at ion impact energies <=100 keV. In fact, as mentioned before the ion sputtering yields increase with energy, especially for heavy ions (*Cassidy et al., 2012*) which are expected in Ganymede's environment (*Mauk et al., 2004; Cooper et al., 2001*). Even if the extrapolated ion-sputtering yields could be overestimated since the ion impact at these high energies could be a more-complex process including implantation, for sure some additional particle release could be produced. From a rough evaluation, the inclusion of the energies up to 1 MeV could produce a particle release of the same order of magnitude of the already simulated one. We decide to limit our simulations at the energies where yields are documented with real laboratory measurements since the inclusion of the higher-energies ion impacts would not change the order of magnitude of the release nor the main results of the paper.

In our simulations of the H_2O and O_2 exosphere we considered a temperature dependent release rate varying between the day and night side of the moon surface. However, Ganymede passes through the Jupiter's shadow and as a result the moon surface can cool down up to the minimum temperature (~80 K). This could have an important effect on the sublimation and the radiolysis rate. *Turc et al. (2014)* have demonstrated that all sublimated water should disappear when Ganymede is in the shadow of Jupiter. A similar effect could be reproduced also by our model since such a

dramatic temperature decrease would cause a 2 orders of magnitude decrease of the O_2 release yield. However, this effect is expected to influence the high altitude density profile, since the multiple bouncing of the O_2 molecules near the surface distributes the gas almost homogeneously at low altitudes.

5 Summary and conclusions

In order to describe the spatial distribution of the H_2O and O_2 exospheric densities around Ganymede, we have firstly simulated the plasma entry and circulation inside Ganymede's magnetosphere, using the global MHD model of Ganymede's magnetosphere (*Jia et al., 2009)*. Then, we developed a 3D MC particle model that for the first time takes into consideration the inhomogeneity of the plasma impact on the surface of Ganymede, determined by the morphology of the moon's intrinsic magnetic field. The assumed exospheric sources are sputtering and sublimation, for H_2O, and radiolysis of the surface water molecules, for O_2; collisions between neutrals and ions or between neutrals themselves are not taken into account.

The results of our study refer to a specific configuration where Ganymede is in the center of JPS with its leading hemisphere illuminated. They can be summarized as follows:

- the plasma precipitation at Ganymede occurs mainly in a region related to the OCFB location with an extent that depends on the plasma mirroring rate in Jupiter's magnetosphere;
- at small altitudes above the moon's subsolar point the main contribution to the neutral environment comes from sublimated H_2O;
- the spatial distribution of the directly sputtered-H_2O molecules exhibits a close correspondence with the plasma precipitation region and extends at high altitudes, being, therefore, well differentiated from the sublimated water ;
- the O_2 exosphere comprises an homogeneous, relatively dense, close to the surface thermal-O_2 region and a less homogeneous part consisting of more energetic O_2 molecules resulting from direct surface sputtering, with a spatial distribution that depends both on the plasma surface impact and surface temperature;
- the O_2 column densities derived by our model at the Sun-moon and anti-Sun-moon directions in the equatorial plane are $4.2 \cdot 10^{17}$ m^{-2} and $3.9 \cdot 10^{17}$ m^{-2}.

respectively, slightly lower than estimations based on the HST observations; possible explanation is the energy upper limit of our simulated ions;

- the assumption of plasma non-mirroring in the polar cap regions leads to a small decrease of the H_2O and O_2 exospheric densities resulting also in small changes in the overall geometry;
- in the full mirroring assumption, the primary surface sputtering mechanism at the whole polar cap of Ganymede can alone explain the observed higher albedo of this region; in the non-mirroring assumption the polar cap brightness above the OCFB ring can be explained with the action of secondary sputtering due to ionized exospheric particles re-impacting the surface;
- the H_2O and O_2 escape rates calculated with our model are~ $1.2 \cdot 10^{25}$ $s^{-1}$and ~$4.2 \cdot 10^{26}$ s^{-1} respectively, in general agreement with the estimations by other models.

The effort presented in this paper is a first-order tool that can contribute in interpreting the available data, providing numerical information on the exospheric density distributions in the vicinity of Ganymede and estimations of the oxygen and water escape rates from the moon. However, more detailed observations of Ganymede's environment are needed in order to provide more accurate model constraints. New experimental data can be of great help for simulations and they are urgently needed. Inclusion of ion-neutrals collisions in our model is intended for the near future. The simulation results in this analysis can be of help for the planning of the future Jupiter Icy moon Explorer (JUICE) mission.

References

Andersen, H., Bay, H.L., 1981. In: Behrisch, R. (Ed.), Sputtering by Particle Bombardment I. Springer-Verlag, Berlin. (Chapter 4).

Bagenal, F., 1994. Empirical model of the Io plasma torus: Voyager measurements, J. Geophys. Res. 99, 11,043–11,062.

Benyoucef, D., Yousfi, M., 2014. Ar+/Ar, O2+/O2 and N2+/N2 Elastic Momentum Collision Cross Sections: Calculation and Validation Using the Semi-Classical Model, Plasma Science and Technology, Vol. 16, No. 6.

Barth, C.A., Hord, C.W., Stewart, A.I.F., Pryor, W.R., Simmons, K.E., McClin- tock, W.E., Ajello, J.M., Naviaux, K.L., Aiello, J.J., 1997. Galileo Ultraviolet

Spectrometer observations of atomic hydrogen in the atmosphere of Ganymede. Geophys. Res. Lett. 24, 2147–2150.

Boring, J.W., Garrett, J.W., Cummings, T.A., Johnson, R.E., Brown, W.L., 1984. Sputtering of solid SO2. Nucl. Instrum. Methods B 1, 321–326.

Broadfoot, A.L., Sandel, B.R., Shemansky, D.E., McConnell, J.C., Smith, G.R., Holberg, J.B., Atreya, S.K., Donahue, T.M., Strobel, D.F., Bertaux, J.L. et al., 1981. Overview of the Voyager ultraviolet spectrometry results through Jupiter encounter. J. Geophys. Res. 86, 8259–8284., http://dx.doi.org/10.1029/JA086iA10p08259.

Brown, W.L., Augustyniak, W.M., Marcantonio, K.J., Simmons, E.H., Boring, J.W., Johnson, R.E., Reimann, C.T., 1984. Electronic sputtering of low temperature molecular solids. Nucl. Instrum. Methods Phys. Res. B 1, 307–314.

Brown, W.L., Johnson, R.E., 1986. Sputtering of ices, a review. Nucl. Instrum. Methods B 13, 295–303.

Brown, M. E., Observation of mass loading in the Io plasma torus, Geophys. Res. Lett. 21, 847–850, 1994.

Burger, M.H., Wagner, R., Jaumann, R., Cassidy, T.A., 2010. Effects of the External Environment on Icy Satellites, Space Science Reviews, June 2010, Volume 153, Issue 1-4, pp 349-374

Cassidy, W., Johnson, R.E., 2005. Monte Carlo model of sputtering and other ejection processes within a regolith. Icarus 176, 499–507.

Cassidy, T.A., Johnson, R.E., McGrath, M.A., Wong, M.C., Cooper, J.F., 2007. The spatial morphology of Europa's near-surface O2 atmosphere. Icarus 191, 755–764.

Cassidy, T., Coll, P., Raulin, F., Carlson, R.W., Johnson, R.E., Loeffler, M.J., Hand, K.P., Baragiola, R.A., 2010. Radiolysis and photolysis of icy satellite surfaces: experiments and theory. Space Science Reviews 153 (1–4), 299–315.

Cassidy, T.A., et al., Paranicas, C.P., Shirley, J.H., Dalton, J.B., Teolis, B.D., Johnson, R.E., Kamp, L., Hendrix, A.R., 2012. Magnetospheric ion sputtering and water ice grain size at Europa. Planetary and Space Science, http://dx.doi.org/10.1016/j.pss.2012.07.008

Cooper, J.F., Johnson, R.E., Mauk, B.H., Garrett, H.B., Gehrels, N., 2001. Energetic ion and electron irradiation of the icy galilean satellites. Icarus 149, 133-159.

Eviatar, A., Williams, D.J., Paranicas, C., McEntire, R.W., Mauk, B.H., Kivelson, M.G., 2000. Trapped energetic electrons in the magnetosphere of Ganymede. J. Geophys. Res. 105, 5547–5553.

Eviatar, A., Strobel, D.F., Wolven, B.C., Feldman, P.D., McGrath, M.A., Williams, D.J., 2001a. Excitation of the Ganymede Aurora. Astrophys. J. 555, 1013–1019.

Eviatar, A., Vasyliunas, V.M., Gurnett, D.A., 2001b. The ionosphere of Ganymede. Planet. Space Sci. 49, 327–336. http://dx.doi.org/10.1016/S00320633(00)00154-9, 2001b.

Famà, M., Shi, J., Baragiola, R.A., 2008. Sputtering of ice by low-energy ions. Surf. Sci. 602, 156–161.

Feldman, P.D., McGrath, M.A., Strobel, D.F., Warren Moos, H., Retherford, K.D., Wolven, B.C., 2000. HST/STIS ultraviolet imaging of polar aurora on Ganymede. Astrophys. J. 535, 1085–1090.

Frank, L. A. and W. R. Paterson, 2001. Survey of thermal ions in the Io plasma torus with the Galileo spacecraft, J. Geophys. Res. 106, 6131–6150.

Frank, L. A., W. R. Paterson, K. L. Ackerson, and S. J. Bolton (1997), Outflow of hydrogen ions from Ganymede, Geophys. Res. Lett., 24(17), 2151 – 2154.

Gurnett, D.A., Kurth, W.S., Roux, A., Bolton, S.J., Kennel, C.F., 1996. Evidence for a magnetosphere at Ganymede from plasma-wave observations by the Galileo spacecraft. Nature 384 (6609), 535–537. http://dx.doi.org/10.1038/384535a0.

Hall, D.T., Strobel, D.F., Feldman, P.D., McGrath, M.A., Weaver, H.A., 1995. Detection of an oxygen atmosphere on Jupiter's moon Europa. Nature 373, 677–679. http://dx.doi.org/10.1038/373677a0.

Hall, D.T., Feldman, P.D., McGrath, M.A., Strobel, D.F., 1998. The far ultraviolet oxygen airglow of Europa and Ganymede. Astrophys. J. 499, 475–481.

Haring, R.A., Pedrys, R., Oostra, D.J., Haring, A., de Vries, A.E., 1984. Reactive sputtering of simple condensed gases by keV ions. III. Kinetic energy distributions. Nucl. Instrum. Methods B 5, 483–488.

Hofer, W.O., 1991. Angular, energy, and mass distribution of sputtered particles. In: Behrisch, R., Wittmaack, K. (Eds.), Sputtering by Particle Bombardment. Springer, Berlin, pp. 15–90.

Itikawa, Y., Mason, N., 2005. Cross Sections for Electron Collisions with Water Molecules, J. Phys. Chem. Ref. Data 34, 1–22

Jia, X., Walker, R.J., Kivelson, M.G., Khurana, K.K., Linker, J.A., 2008. Three dimensional MHD simulations of Ganymede's magnetosphere, Journal of Geophysical Research, 113, A06212, doi:10.1029/2007JA012748.

Jia, X., Walker, R.J., Kivelson, M.G., Khurana, K.K., Linker, J.A., 2009. Properties of Ganymede's magnetosphere inferred from improved three-dimensional MHD simulations. Journal of Geophysical Research, 114, A09209, doi:10.1029/2009JA014375.

Jia, X., R. J. Walker, M. G. Kivelson, K. K. Khurana and J. A. Linker, 2010. Dynamics of Ganymede's magnetopause: Intermittent reconnection under steady external conditions, Journal of Geophysical Research, 115, A12202, doi:10.1029/2010JA015771.

Johnson, R.E., 1990. Energetic charged-particle interactions with atmospheres and surfaces. Springer-Verlag eds. ISBN 3-540-51908-4 Berlin Heidelberg New York; ISBN 0-387-51908-4 new York Berlin Heidelberg

Johnson, R.E., 1997. Polar caps on Ganymede and Io revisited. Icarus 128, 469–471. http://dx.doi.org/10.1006/icar.1997.5746.

Johnson, R.E., 2001. Surface chemistry in the jovian magnetosphere radiation environment. In: Dessler, R. (Ed.), Chemical Dynamics in Extreme Environments. Adv. Ser. Phys. Chem. World Scientific, Singapore 11, pp. 390–419 (Chapter 8).

Johnson, R.E., Lanzerotti, L.J., Brown, W.L., Armstrong, T.P., 1981. Erosion of Galilean satellites by magnetospheric particles. Science 212, 1027–1030.

Johnson, T.V., Soderblom, L.A., Mosher, J.A., Danielson, G.H., Cook, A.F., Kupferman, P.N., 1983. Global multispectral mosaics of the icy Galilean satellites. Journal of Geophysical Research 88, 5789–5805.

Johnson, R. E., Liu, M., & Tully, C. 2002. Collisional Dissociation Cross Section for O + O2, CO and N2 and N + N2. Planet. Space Sci., 50, 123.

Johnson, R.E., Carlson, R.W., Cooper, J.F., Paranicas, C., Moore, M.H., Wong, M.C., 2004. Radiation effects on the surfaces of the Galilean satellites, in Jupiter. Planet Satellites Magnetosp. 485–512.

Khurana, K., Kivelson, M. G., Vasyliunas, V. M., Krupp, N., Woch, J., Lagg, A., Mauk, B.H., and Kurth, W.S., 2004. The Configuration of Jupiter's Magnetosphere. in Jupiter: The Planet, Satellites and Magne- tosphere, Chap. 24, edited by. F. Bagenal, T. Dowling, W. McKinnon, Cambridge University Press.

Khurana, K.K., Pappalardo, R.T., Murphy, N., Denk, T., 2007. The origin of Ganymede's polar caps. Icarus 191, 193–202. http://dx.doi.org/10.1016/ j.icarus.2007.04.022.

Kivelson, M.G. et al., 1996. Discovery of Ganymede's magnetic field by the Galileo spacecraft. Nature 384, 537–541.

Kivelson, M.G., Khurana, K.K., Coroniti, F.V., Joy, S., Russell, C.T., Walker, R.J., Warnecke, J., Bennett, L., Polanskey, C., 1997. The magnetic field and magnetosphere of Ganymede. Geophysical Research Letters 24, 2155–2158.

Kivelson, M.G., Warnecke, R.J., Bennett, J., Joy, S., Khurana, K.K., Linker, J.A., Russell, C.T., Walker, J., Polanskey, C., 1998. Ganymede's magnetosphere: magnetometer overview. Journal of Geophysical Research 103, 19963–19972.

Kivelson, M. G., F. Bagenal, W. S. Kurth, F. M. Neubauger, C. Paranicas, and J. Saur (2004), Magnetospheric interactions with satellites, in Jupiter: The Planet, Satellites and magnetosphere, edited by F. Bagenal, T. E. Dowling, and W. B. McKinnon, pp. 513 – 536, Cambridge Univ. Press, Cambridge, U. K.

Kliore, A. J., Satellite atmospheres and magnetospheres, High- lights in Astronomy 11, 1065, 1998.

Krishnakumar, E., Srivastava, S.K., 1992. Cross sections for electron impact ionization of O2. Int. J. Mass Spectrom. Ion. 113, 1–12.

Lagg, A., Krupp, N., Woch, J., Williams, D.J., 2003. In situ observations of a neutral gas torus at Europa. Geophys. Res. Lett. 30, 110000–110001.

Luna, H., McGrath, C., Shah, M.B., Johnson, R.E., Liu, M., Latimer, C.J., Montenegro, E.C., 2005. Dissociative charge exchange and ionization of O2 by Fast H+ and O+ ions: energetic ion interactions in europa's oxygen atmosphere and neutral torus. Astrophysical Journal 628 (2), 1086–1096.

Marconi, M.L., 2007. A kinetic model of Ganymede's atmosphere, x Icarus 190 (2007) 155–174.

Mauk, B. H., Gary, S. A., Kane, M., Keath, E.P., Krimigis, S.M., Armstrong, T.P., 1996. Hot plasma parameters of Jupiter's inner magnetosphere, Journal of Geophysical Research, Volume 101, Issue A4, p. 7685-7696.

Mauk, B.H., Mitchell, D.G., Krimigis, S.M., Roelof, E.C., Paranicas, C.P., 2003. Energetic neutral atoms from a trans-Europa gas torus at Jupiter. Nature 421 (6926), 920–922.

Mauk, B.H., Mitchell, D.G., McEntire, R.W., Paranicas, C.P., Roelof, E.C., Williams, D.J., Krimigis, S.M., Lagg, A., 2004. Energetic ion characteristics and neutral gas interactions in Jupiter's magnetosphere. Journal of Geophysical Research 109, A09S12.

McGrath, M.A., Lellouch, E., Strobel, D.F., Feldman, P.D., Johnson, R.E., 2004. Satellite atmospheres. In: Bagenal, F., Dowling, T.E., McKinnon., W.B. (Eds.), Jupiter. The planet, Satellites and Magnetosphere. Cambridge Planetary Science, 1. Cambridge University Press, Cambridge, UK, ISBN: 0-521-81808-7, pp. 457–483.

McGrath, M.A., Xianzhe, J., Retherford, K., Feldman, P.D., Stroberl, D.F., Saur, J., 2013. Aurora on Ganymede , Journal of Geophysical Research: Space Physics, Volume 118, Issue 5, pp. 2043-2054

McNutt, R. L., J. W. Belcher, and H. S. Bridge, Positive ion obser- vations in the middle magnetosphere of jupiter, J. Geophys. Res. 86, 8319, 1981.

Morrison, D. and J. Samz, Voyage to Jupiter, NASA, 1980.

Mura, A., Wurz, P., Lichtenegger, H.I.M., Schleicher, H., Lammer, H., Delcourt, D., Milillo, A., Orsini, S., Massetti, S., Khodachenko, M.L., 2009. The sodium exosphere of Mercury: Comparison between observations during Mercury's transit and model results. Icarus 200, 1–11.

Orton, G.S., Spencer, J.R., Travis, L.D., Martin, T.Z., Tamppari, L.K., 1996. Galileo photopolarimeter–radiometer observations of Jupiter and the Galilean satellites. Science 274, 389–392.

Paranicas, C., Paterson, W.R., Cheng, A.F., Mauk, B.H., McEntire, R.W., Frank, L.A., Williams, D.J., Energetic particle observations near Ganymedeet al., 1999. Journal of Geophysical Research 104, 17459–17469.

Paterson, W. R., L. A. Frank, and K. L. Ackerson, Galileo plasma observations at Europa: Ion energy spectra and moments, J. Geophys. Res. 104, 22,779–22,792, 1999.

Paty, C., and R. Winglee (2004), Multi-fluid simulations of Ganymede's mag- netosphere, Geophys. Res. Lett., 31, L24806, doi:10.1029/2004GL021220.

Pilcher, C.B., Ridgway, S.T., McCord, T.B., 1972. Galilean satellites: Identification of water frost. Science 178, 1087–1089. http://dx.doi.org/10.1126/science. 178.4065.1087.

Plainaki, C., Milillo, A., Mura, A., Orsini, S., Cassidy, T., 2010. Neutral particle release from Europa's surface. Icarus 210, 385–395.

Plainaki, C., Milillo, A., Mura, A., Orsini, S., Massetti, S., Cassidy, T., 2012. The role of sputtering and radiolysis in the generation of Europa exosphere. Icarus 218 (2), 956–966, http://dx.doi.org/10.1016/j.icarus.2012.01.023.

Plainaki, C., Milillo, A., Mura, A., Orsini, S., Saur, 2013. Exospheric O2 densities at Europa during different orbital phases, Planetary and Space Science, Volume 88, p. 42-52. http://dx.doi.org/10.1016/j.pss.2013.08. 011

Pospieszalska, M.K., Johnson, R.E., 1989. Magnetospheric ion bombardment profiles of satellites: Europa and Dione. Icarus 78, 1–13.

Purves, N.G., Pilcher, C.B., 1980. Thermal migration of water on the Galilean satellites. Icarus 43, 51–55. http://dx.doi.org/10.1016/0019-1035(80)90086-X.

Reimann, C.T., Boring, J.W., Johnson, R.E., Garrett, L.W., Farmer, K.R., 1984. Ion-induced molecular ejection from D_2O ice. Surface Science 147, 227–240.

Roosendaal, H.E., Hating, R.A., Sanders, J.B., 1982. Surface disruption as an observable factor in the energy distribution of sputtered particles. Nucl. Instrum. Methods 194, 579–581.

Saur, J., Strobel, D.F., Neubauer, F.M., 1998. Interaction of the Jovian magnetosphere with Europa: constraints on the neutral atmosphere. Journal of Geophysical Research 103, 19947–19962.

Scudder, J. D., E. C. Sittler, and H. S. Bridge, 1981. A survey of the plasma electron environment of Jupiter - A view from Voy- ager, J. Geophys. Res. 86, 8157–8179.

Shi, J., Teolis, B.D., Baragiola, R.A., 2007. Irradiation enhanced adsorption and trapping of O2 on microporous waterice. Bulletin of the American Astronomical Society 38, 489.

Smith, B. A., Soderblom, L.A., Beebe, R., Boyce, J., Briggs, G., Carr, M., Collins, S.A., Cook II, A.F., Danielson, G.E., Davies, M.E., Hunt, G.E., Ingersoll, A., Johnson, T.V., Masursky, H., McAuley, J., Morrison, D., Owen, T., Sagan, C., Shoemaker, E.M., Strom, R., Suomi, V.E., Veverka, J., 1979. Galilean satellites and Jupiter—Voyager 2 imaging science results, Science 206, 927–950.

Scudder, J.D., Sittler, E.C., Bridge, H.S., 1981. A survey of the plasma electron environment of Jupiter - A view from Voyager, Journal of Geophysical Research 86, 8157-8179.

Sigmund, P., 1969. Theory of sputtering. I. Sputtering yield of amorphous and polycrystalline targets. Phys. Rev. 184, 383–416.

Shematovich, V.I., Johnson, R.E., Cooper, J.F., Wong, M.C., 2005. Surface-bounded atmosphere of Europa. Icarus 173, 480–498.

Smyth, W.H., Marconi, M.L., 2006. Europa's atmosphere, gas tori, and magnetospheric implications. Icarus 181, 510–526.

Spencer, J.R., Tamppari, L.K., Martin, T.Z., Travis, L.D., 1999. Temperatures on Europa from Galileo photopolarimeter–radiometer: Nighttime thermal anomalies. Science 284, 1514–1516.

Smyth, W.H., Marconi, M.L., 2006. Europa's atmosphere, gas tori, and magnetospheric implications. Icarus 181, 510–526.

Straub, H.C., P. Renault, B.G. Lindsay, K.A. Smith, R.F. Stebbings, 1996. Phys. Rev. A 54, 2146–2153

Teolis, B.D., Jones, G.H., Miles, P.F., Tokar, R.L., Magee, B.A., Waite, J.H., Roussos, E., Young, D.T., Crary, F.J., Coates, A.J., Johnson, R.E., Tseng, W.-L., Baragiola, R.A., 2010. Cassini finds an oxygen-carbon dioxide atmosphere at Saturn's Icy Moon Rhea. Science 330, 1813–1815.

Thomas, N., G. Lichtenberg, and M. Scotto, 2001. High-resolution spec- troscopy of the Io plasma torus during the Galileo mission, J. Geophys. Res. 106, 26,277–26,292.

Turc, L., Leclercq, L., Leblanc, F., Modolo, R., Chaufray, J.-Y., 2014. Modelling Ganymede's neutral environment: A 3D test-particle simulation. Icarus 229, 157-169.

Turner, B. R., Rutherford, J.A., 1968. Charge transfer and ion-atom interchange reactions of water vapor ions, J. Geophys. Res. 73, 6751

Vasyliunas, V. M. and A. Eviatar, 2000. Outflow of ions from Ganymede: a reinterpretation, Geophys. Res. Lett. 27, 1347.

Watson, C.C., Tombrello, T.A., 1983. Band-Aid Report, Cal. Tech. Pasadena, CA.

Williams, D.J., Mauk, B.H., McEntire, R.W., 1997. Trapped electrons in Ganymede's magnetic □eld. Geophys. Res. Lett. 24, 2953–2956.

Williams, D.J., Mauk, B.H., McEntire, R.W., 1998. Properties of Ganymede's magnetosphere as revealed by energetic particle observations. J. Geophys. Res. 103, 17,523–17,534.

Williams, D. J., 2001. Energetic particle environment in the Jovian magnetosphere, in Conf. on Magnetospheres of the Outer Planets, p. 19, (Paris, France).

Yung, Y.L., McElroy, M.B., 1977. Stability of an oxygen atmosphere on Ganymede. Icarus 30, 97–103. http://dx.doi.org/10.1016/0019-1035(77)90124-5.

Figures

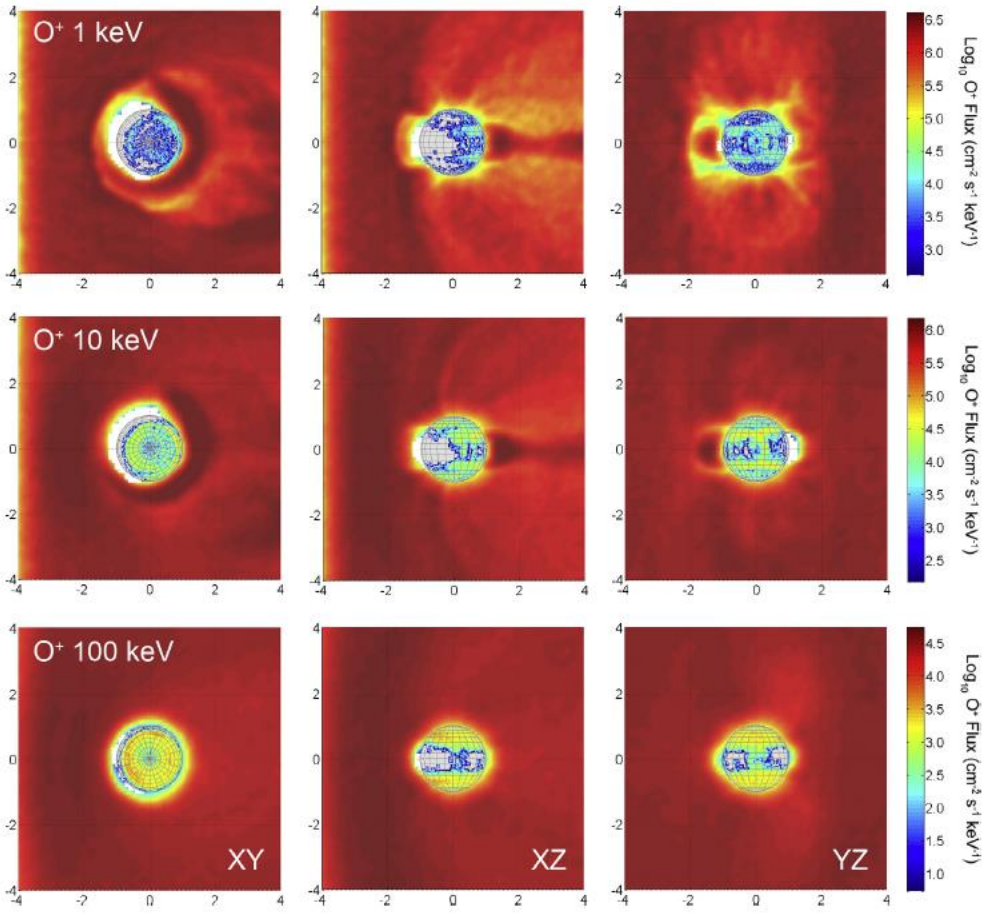

Figure 1: *O^+ differential flux ($cm^{-2}\ s^{-1}\ sr^{-1}\ keV^{-1}$) around Ganymede at initial energy equal to 1 keV (first row), 10 keV (second row), 100 keV (third row). X is along the ambient flow direction (and Ganymede's orbital motion), Z is along the Jupiter's spin axis, and Y points toward Jupiter (in units of Ganymede's radii). First column shows the XY-, second column XZ- and third column YZ-projections.*

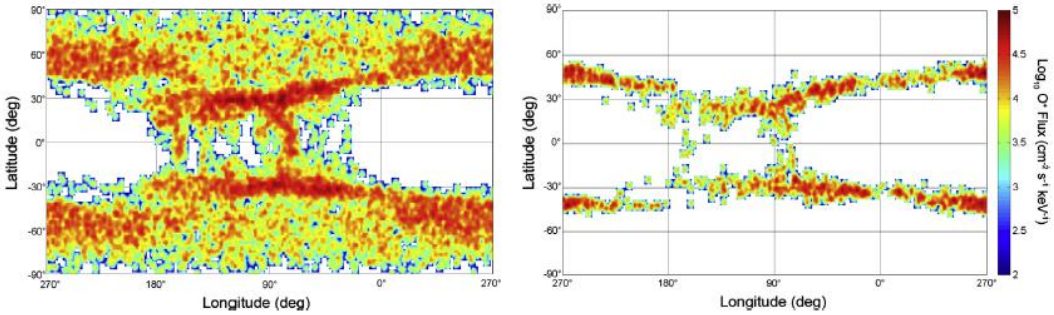

Figure 2: *Precipitation map of the O^+ differential flux ($cm^{-2}\ s^{-1}\ sr^{-1}\ keV^{-1}$) around Ganymede at initial energy equal to 10 keV in the full mirroring (left) and non-mirroring (right) assumption. Jupiter is at 0° longitude, leading at 90°. The colorbar scale is logarithmic.*

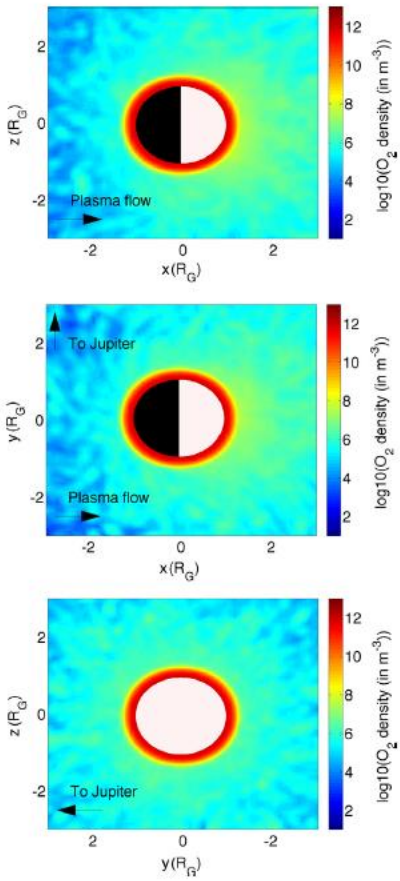

Figure 3: *The O_2 exosphere of Ganymede generated due to the radiolytic decomposition of ice being impacted by Jupiter's magnetospheric ions to (S^+, O^+ and H^+). Top panel shows the exospheric density distribution at the XZ plane (X is along the ambient flow direction and Ganymede's orbital motion and Z is along the Jupiter's spin axis (in units of Ganymede's radii)); middle panel refers to the XY plane (Y points towards Jupiter (in unit of Ganymede's radii)); bottom panel shows the trailing hemisphere exosphere in the YZ plane.*

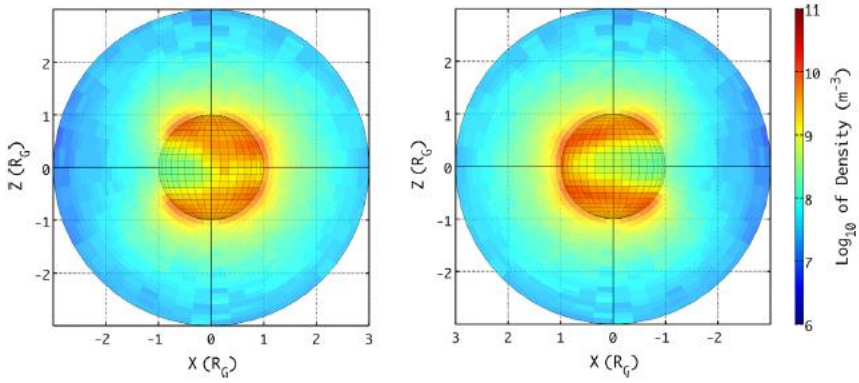

Figure 4: *XZ projection of the sputtered H_2O density. X is along the ambient flow direction (and Ganymede's orbital motion), Z is along the Jupiter's spin axis, and Y points toward Jupiter (in units of Ganymede's radii). In the right panel, the Jupiter-facing hemisphere of Ganymede) is shown (trailing side is on the right). In the left panel the other hemisphere is shown (leading side is on the right).*

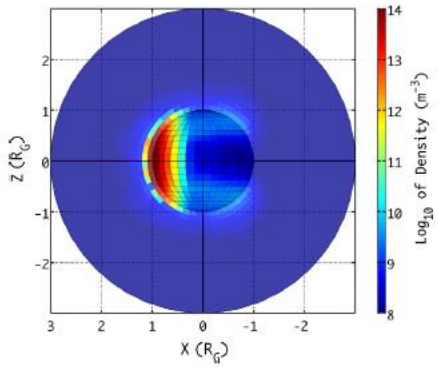

Figure 5: *XZ projection of the H_2O exosphere density due to sublimation and sputtering over the surface of Ganymede. X is along the ambient flow direction (and Ganymede's orbital motion), Z is along the Jupiter's spin axis, and Y points toward Jupiter (in units of Ganymede's radii). The Jupiter-facing hemisphere is shown (the illuminated leading hemisphere is on the left). It is clear that the sputtered exosphere is much less intense close to subsolar point, while it is the major generation process in the rest of the moon.*

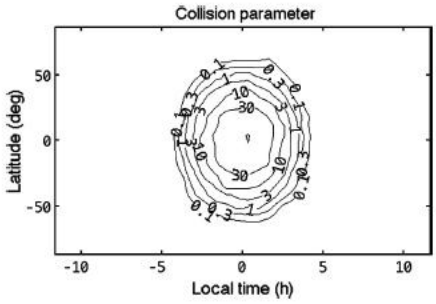

Figure 6: *Contour lines of the inverse of the Knudsen number, calculated at the surface of Ganymede assuming both sources of sputtering and sublimation.*

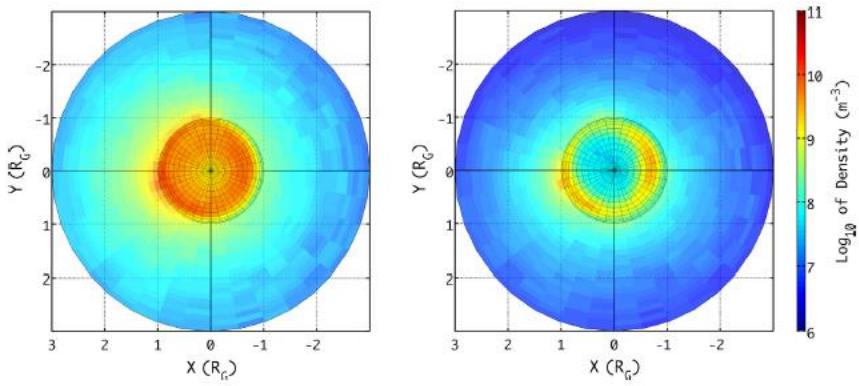

Figure 7: *XY projection of the sputtered H_2O exosphere density due to S^+, O^+ and H^+ impact in the full mirroring (left) and non-mirroring (right) assumptions. X is along the ambient flow direction (and Ganymede's orbital motion), Z is along the Jupiter's spin axis, and Y points toward Jupiter (in units of Ganymede's radii).*

Table Captions

Table 1: *Total precipitating rate for different energy ranges of the ion species impacting Ganymede's surface (in particles s^{-1}).*

Table 2 : *H_2O Sputtering yield for different energies and species of precipitating ions.*

Table 3*: Plasma and orbital parameters of Ganymede (adapted from Table 21.1 in Kivelson et al., 2004)*

Table 4: *O_2 and H_2O exospheres loss rates at Ganymede*

Table 5*: Comparison of the O_2 exospheric densities derived from different models*

Tables

Table *1*

Energy range (keV)	**H^+**	**O^+**	**S^+**
<3	$2.4 \cdot 10^{22}$	$1.1 \cdot 10^{22}$	$1.1 \cdot 10^{23}$
3-7.5	$3.4 \cdot 10^{22}$	$3.5 \cdot 10^{22}$	$9.4 \cdot 10^{22}$
7.5-30	$1.3 \cdot 10^{23}$	$1.6 \cdot 10^{23}$	$2.8 \cdot 10^{23}$
30-75	$9 \cdot 10^{22}$	$7.7 \cdot 10^{22}$	$7.8 \cdot 10^{22}$
75-125	$5 \cdot 10^{22}$	$4.1 \cdot 10^{22}$	$5.1 \cdot 10^{22}$
Total	$3.3 \cdot 10^{23}$	$3.2 \cdot 10^{23}$	$6.1 \cdot 10^{23}$

Table 2

Energy (keV)	**H**	**O**	**S**
1	1.3	25	39
5	1.4	36	59
10	1.9	43	67
50	5.3	120	81
100	5.7	260	100

Table 3

Symbol (units), physical property	Value	Reference	Note
n_e (elns cm^{-3}), equator average (range) plasma electron density;	5 (1-10)	*Bagenal et al., 1994; Kivelson et al., 2004*	*1*
n_i (ions cm^{-3}), average (range) ion density;	4 (1-8)	*Bagenal et al., 1994; Kivelson et al., 2004*	*1*
kT_e (eV) plasma electron thermal energy;	300	*Scudder et al., 1981*	*2*
kT_i (eV), equator average (range) plasma ion energy	60 (10-100)	*Bagenal et al., 1994; Kivelson et al., 2004*	*1*
v_s (km s^{-1}), satellite orbital velocity	11		
v_φ (km s^{-1}), plasma azimuthal velocity (range);	150 (95-163)	*Morrison and Samz (1980)*	*1, 3*
u (km s^{-1}), relative velocity (range)	139 (84-152)	*Kivelson et al., 2004*	*1*

Notes on Table *3*

1: The first value of a parameter is the average inferred value in the vicinity of the Jupiter's near-equatorial current sheet. The values in parentheses show the minimum or maximum values measured or inferred, in case the variations were not systematically related to latitude.

2: Effective electron energies (combining thermal and suprathermal components) interpolated from Scudder et al. (1981) and consistent with Paterson et al. (1999) and Frank and Paterson (2001).

3: The plasma azimuthal estimates are the largest reported, likely to reflect the unperturbed flow speeds at the orbits of the moons. Lower values are also observed, especially close to the moons. The range of cited values are based on spectroscopic measurements (Brown, 1994; Thomas et al. 2001) as well as in situ measurements from Williams (2001) for Ganymede.

Table 4

Loss process	Loss rate (s^{-1})	Region in the exosphere	Dens. of the reactant (cm^{-3})	κ (cm^3 s^{-1})	Notes
$e + O_2 \rightarrow O_2^+ + 2e$	$4.5\cdot10^{-7}$ ($9\cdot10^{-8}$ - $9\cdot10^{-7}$)	polar caps	5 (1-10)	$9\cdot10^{-8}$	*1, 2*
$e + H_2O \rightarrow OH + H + e$	$4.8\cdot10^{-7}$ ($9.6\cdot10^{-8}$ - $9.6\cdot10^{-7}$)	polar caps	5 (1-10)	$9.6\cdot10^{-8}$	*1, 3*
$O^+ + O_2 \rightarrow O_2^+ + O$	$3\cdot10^{-8}$ ($8.3\cdot10^{-8}$)	polar caps	$3.3\ 10^2$ (polar caps)	$9\cdot10^{-11}$ ($2.5\cdot10^{-}$	*4, 5*
	$3.3\cdot10^{-8}$ ($9.3\cdot10^{-8}$)	closed			*4, 5*

		field lines	3.7 10^2 (closed field line region)	^{10})	
$O^+ + H_2O$ --> $O + H_2O^+$	1.5 $\cdot 10^{-6}$ (1.7 $\cdot 10^{-6}$)	polar caps		4.5$\cdot 10^{-9}$ (5.3$\cdot 10^{-9}$)	*4, 5*
	1.7 $\cdot 10^{-6}$ (1.9 $\cdot 10^{-6}$)	closed field lines			
$O_2^+ + O_2$ --> $O_2 + O_2^+$	4 $\cdot 10^{-6}$ (5.5 $\cdot 10^{-6}$)	polar caps	2.2 10^3 (polar caps)	1.8$\cdot 10^{-9}$ (2.5$\cdot 10^{-9}$)	*4, 5*
$O_2^+ + H_2O$ --> $O_2 + H_2O^+$	1.6 $\cdot 10^{-5}$ (1.9 $\cdot 10^{-5}$)	polar caps		7.2$\cdot 10^{-9}$ (8.8$\cdot 10^{-9}$)	*4, 5*
$O_2 + hv$ --> $O + O$	1.6$\cdot 10^{-7}$	illuminated hemisphere	-	-	*6*
$H_2O + hv$--> $OH + H$	3.9 $\cdot 10^{-7}$	illuminated hemisphere	-	-	*6*

***Notes on* Table 4**

1: The first value of the electron density parameter is the average inferred value in the vicinity of the Jupiter's near-equatorial current sheet (Bagenal et al., 1994; Kivelson et al., 2004). The values in parentheses show the minimum or maximum values measured or inferred, in case the variations were not systematically related to latitude.

2: The value of κ corresponds to 100 eV electrons and is taken by Itikawa and Mason (2005).

3: The value of κ corresponds to 100 eV electrons and is taken by Straub et al. (1996).

4: Value in parenthesis corresponds to the estimated upper limit of the ion flow velocity (equal to 25 km/s according to Eviatar et al., 2001b).

5: We estimate the rate coefficient, κ, by multiplying the ion flow velocity estimated by Eviatar et al. (2000) and Eviatar et al. (2001b) with the cross section of the reaction, i.e. $\kappa = v_{flow} * \sigma * (v_{flow})$

6: The considered rates are from Huebner et al. (1992).

Table 5

	O_2 density at $h \sim 0.4$ R_G		O_2 density at $h \sim 0.15$ R_G		O_2 density at $h \sim 0.05$ R_G	
	above the SSP	above the poles	above the SSP	above the poles	above the SSP	above the poles
this model	2.6$\cdot 10^7$ m^{-3}	2.8$\cdot 10^6$ m^{-3}	8.2$\cdot 10^{10}$ m^{-3}	8$\cdot 10^{10}$ m^{-3}	1.5$\cdot 10^{12}$ m^{-3}	1.4$\cdot 10^{12}$ m^{-3}
model by *Turc et al. (2014)*	<< 10^9 m^{-3}	<< 10^9 m^{-3}	<< 10^9 m^{-3}	<< 10^9 m^{-3}	~5$\cdot 10^{10}$ m^{-3}	~10^{10} m^{-3}
model by *Marconi (2007)*	~ 10^{10} m^{-3}	~ 10^9 m^{-3}	~ 10^{10} m^{-3}	~ 10^{10} m^{-3}	~10^{10} m^{-3}	~10^{12} m^{-3}